Structural Analysis of the Sambagawa Crystalline Schists of the Sazare Mining District, Central Shikoku

By

Norio ÔYAGI

with 52 Text-figures, 2 Plates, and 2 Tables

ABSTRACT: Rock structures of crystalline schists in the Sambagawa metamorphic zone have been analysed and described in three scales, macroscopic, mesoscopic, and microscopic scales. Relation between these structures and metamorphism has been briefly considered. Gradual change in styles of folds and *S*-surfaces during metamorphism can be recognized. Orientation of fold axes and lineations is variable in the early stages but is constant in the later stages of the Sambagawa metamorphism. Change in movement plan which is suggested from orientation of rock structures during metamorphism has been recognized.

CONTENTS

I. INTRODUCTION

The Sazare mining district is situated 20km east of the Besshi mine in Central Shikoku, being occupied with crystalline schists of the Sambagawa metamorphic zone. The sambagawa metamorphic zone is a narrow zone with width of 30km to 40km and with length of more than 800km from Kanto Province to Kyushu Province. Linear structures in the crystalline schists are not always parallel to the trend of the zone: those parallel to or nearly parallel to the general trend of the Sambagawa zone are observed extensively, while normal to or nearly normal to the zone have been reported from several districts. In Chubu Province, the latter type of linear structures has been reported from the Tenryu River district (NAKAYAMA, 1953, 1954, 1960). In Shikoku Province, it has been reported from the districts of Kôtsu

(Nakayama, 1960; Takeda, 1962; Oshima, Iwasaki, and Nakayama, 1963), Besshi-Shirataki (Hide, Yoshino, and Kojima, 1956; Kojima and Hide, 1957, 1958; Hide, 1961), Motoyasu (Yui, 1960), and Sazare (Takeda, 1954; Horikoshi, 1958; Hirata, 1959; Doi, 1959).

At the gallery of the Sazare mine, Takeda (1954) recognized a lineation plunging steeply to the southwest and obliquely to the regional *b*-lineation which is parallel to the axial trend of the Yakushi anticline and the Tsuneyama syncline, and called it the "Hinouchi (ore zone) lineation". Horikoshi (1958) observed this type of lineation ("abnormal lineation L_2" in his sense) in a broad zone with width of less than 1200m. He considered that the "abnormal lineation L_2 is older than "the general lineation L_1" which is regionally observed. Doi (1959) and Hirata (1959), however, stated that L_1 was formed earlier than L_2. Therefore, the time relation between the two linear structures is controversial in this district.

In the Besshi-Shirataki district, Hide (1961) discriminated three stages of formation for small scale folds, namely, the first, the second, and the third stages of folding. He pointed out that the first stage folding shows an "isoclinal" style with "axial plane parallel to the bedding plane", having been formed during the main stage of mineralization of crystalline schists. In the Sazare district, axes of isoclinal folds with such style often steeply and are discordant with the regional *b*-lineation. Therefore, it must be an important problem to clarify the relation between these isoclinal folds and associated linear structures oblique or normal to the regional trend of the Sambagawa metamorphic zone.

Turner (1957) said, "tectonic stream might commonly be directed oblique to the trend of the zone of crustal weakness (orogen) ···. In upper levels ···, it yields by recumbent folding and thrusting across horizontal or gently plunging axis, ··· but at deeper levels movement is constrained to directions more nearly parallel to the length of the orogen. Here transverse folds and related movements across axes that commonly plunge steeply characterized the movement plan." Recently, it has been pointed out that metamorphic conditions of the Sambagawa zone are characterized by high pressure. Miyashiro (1959) suggested that the Sambagawa metamorphism occurred in a very deep place. Can the problem related to the oblique lineation in the Sambagawa metamorphic zone be solved by the term of level of metamorphism as suggested by Turner? The oblique lineations are mostly found in the upper stratigraphical levels in Shikoku. Kojima and Hide (1958) stated, "the extent of axial elongation must be different according to the difference in metamorphic grade or metamorphic behavier of respective zones in a schist or gneiss zone. This difference may give rise to strong lateral displacement, in which transverse linear structure will predominate." For discussion on these statements, one should clarify the relation between tectonic history and metamorphism.

In this paper, the present author intends firstly to analyze and describe rock structures in macroscopic, mesoscopic, and microscopic scales. Secondly, he intends to

clarify the tectonic history of crystalline schists and the meaning of the linear structures oblique to or normal to the regional trend of the Sambagawa zone in this district.

Acknowledgements: The author whishes to record his sincere gratitude to Prof. G. KOJIMA for his kind advices and encouragement throughout the work. The author is also indebted to him for critical reading of the manuscript. Thanks also due to the Drs. K. HIDE, G. YOSHINO, H. YOSHIDA, T. NUREKI and I. HARA and Mr. M. NAKAGAWA for valuable suggestions and discussions. The author expresses his sincere gratitude to the staffs of the Sazare mine, Sumitomo Metal Mining Co. Ltd., Messers Y. OKITA, S. KOIZUMI, N. KANO, Y. HIRATA, J. ISHIKAWA, K. ODA, M. OBARA and H. FUKUDA. He is also indebted to Mr. H. TAKAHASHI who prepared thin sections and Messers H. NAKANO, U. NISHIMURA, N. UCHISETO, and H. IWATA for drawing figures. This study was supported by the Grant in Aid for Scientific Researches from the Ministry of Education of Japan.

II. OUTLINE OF GEOLOGY

A. GEOLOGIC SETTING

In Shikoku, the Sambagawa metamorphic zone is relatively wide, situated between the Median Dislocation Line to the north and the Kamiyakawa-Ikegawa Tectonic Line to the south. General trend of the zone is ENE-WSW. Several major folds have been recognized: the Oboke anticline, the Koboke syncline, the Yakushi anticline, the Tsuneyama syncline, the Nakashichiban anticline, and the Shirataki recumbent fold (Fig. 1) (KOJIMA, 1951; HIDE, YOSHINO and KOJIMA, 1956). Axes of these folds

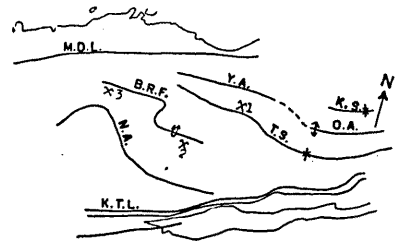

FIG. 1 Structural map of Central Shikoku (after KOJIMA and HIDE; 1958)
O. A.: Oboke anticline.
K. S.: Koboke sycnline.
Y. A.: Yakushi anticline.
T. S.: Tsuneyama syncline.
B. R. F.: Besshi recumbent folds.
N. A.: Nakashichiban anticline.
M. D. L.: Median Dislocation Line.
K. T. L.: Kiyomizu Tectonic Line.
1: Sazare Mine. 2: Shirataki Mine. 3: Besshi Mine.

trend generally ENE-WSW to ESE-WNW. The Yakushi anticline and the Tsuneyama syncline are important macroscopic structures in the Sazare district. The axial trend of the Yakushi anticline is nearly E-W and that of the Tsuneyama syncline varies from E-W to NW-SE as shown in Fig. 1. The Sazare mine is situated on the limb between the two major structures. Rocks of upper stratigraphical horizons show higher metamorphic grade than those of lower horizons. The former has been called spotted schists by characteristic occurrence of albite porphyroblasts and the latter has been named non-spotted schists. In the Sazare district, spotted schists occupy northern, southern and western parts of the district but in central and eastern parts non-spotted schists are distributed.

B. Stratigraphy

In Central Shikoku, the statigraphy of the Sambagawa crystalline schists was set up by Ogawa (1902). Ozawa (1926) considered that there are major recumbent structures in Central Shikoku. Detailed stratigraphy has been established in the Oboke district by Kojima (1951), in the west of the Besshi district by Yoshino and Kojima (1953), and in the Shirataki district by Hide (1954). Kojima, Hide, and Yoshino (1956) summarized and revised the stratigraphy as shown in Table 1.

Table 1. Stratigraphy of the Sambagawa Crystalline Schists in Central Shikoku.

<table>
<tr><th colspan="4">Oboke, Besshi-Shiratrki Districts
(Kojima, Hide and Yoshino; 1956)</th><th colspan="2">Besshi-Sazare Districts
(Doi; 1961)</th><th colspan="2">Sazare District
(Oyagi; 1964)</th></tr>
<tr><td rowspan="6">Yoshinogawa group</td><td>Upper subg.*</td><td colspan="2">Ojoin f.*</td><td colspan="2">Tomisato f.</td><td colspan="2">Ojoin f.</td></tr>
<tr><td rowspan="4">Middle subg.</td><td rowspan="3">Minawa f.</td><td>Upper m.*</td><td rowspan="3">Minawa f.</td><td>Upper m.</td><td rowspan="3">Minawa f.</td><td>Upper m.</td></tr>
<tr><td>Main greenschist m.</td><td>Middle m.</td><td>Middle m.</td></tr>
<tr><td>Lower m.</td><td>Lower m.</td><td>Lower m.</td></tr>
<tr><td colspan="2">Koboke f.</td><td colspan="2">Koboke f.</td></tr>
<tr><td rowspan="2">Lower subg.</td><td colspan="2">Kawaguchi f.</td><td colspan="2">Kawaguchi f.</td></tr>
<tr><td colspan="2">Oboke f.</td><td colspan="2">Oboke f.</td></tr>
<tr><td colspan="4">~~~~~ ? ~~~~~</td><td colspan="2"></td><td colspan="2"></td></tr>
<tr><td>Nishi-iya group</td><td colspan="4"></td><td colspan="2"></td><td colspan="2"></td></tr>
</table>

* subg: subgroup, f: formation, m: member.

In the Besshi-Sazare district, Doi (1959, 1961) has reported the stratigraphy (Table 1). The crystalline schists of the Sazare district can be divided as shown in Table 1.

1. *The Minawa formation*

The lower member. This member can be divided into two parts. The lower part is chiefly composed of pelitic schists with a few thin (5～10 m) layers of basic schists and psammitic schists. The upper part is characterized by thick psammitic schists (100–400 m) with several thin layers of pelitic schists.

The middle member. Pelitic schists are predominant throughout the member. However, a few layers of basic schists are interbedded in the lower part and they are 10 m to 20 m in thickness. These basic schist layers are fairly continuous and bear occasionally bedded cupriferous iron deposits (the Yakushi ore body, the Yokoyabu ore body, and so on). As can be judged from geological maps of Ehime and Kochi prefecture, these basic schist layers are considered to correspond to the main green-schists member in the Besshi-Shirataki district (KOJIMA, HIDE and YOSHINO, 1956). In the upper part, thin layers of psammitic schists are intercalated with pelitic schist.

The upper member. The member is characterized by alternating layers of basic, siliceous and pelitic schists. In the lower part, basic schists or siliceous schist layers are thin (5–10 m), while in the upper part they are thick (10～100 m). Basic schists of this member often bear large bedded cupriferous sulfide ore deposits such as the Sazare ore deposit and the Iyadani ore body. Albite porphyroblasts can be observed from the rocks of this member.

2. *The Ojoin formation*

The formation is chiefly composed of spotted pelitic schist, and intercalated thin layers (1～5 m) of basic, siliceous, and psammitic schists. In some localities, very thin layers (5–10 cm) of calcareous schist are observed. Grain size of albite porphyroblasts is usually large (1～10 m) in this formation.

3. *Correlation*

According to DOI (1959, 1961), the thick layers of psammitic schists of this district are called the Koboke formation. These beds are, however, considered to be identical with the lower member of the Minawa formation, because basic schists are corelated to those of the main green-schist member in Central Shikoku (KOJIMA, HIDE and YOSHINO, 1956).

The thickness of the basic schists in this district is fairly thinner than in other districts in Central Shikoku.

C. GEOLOGIC STRUCTURE

1. *Folds*

The Yakushi anticline can be considered as the continuation of the Oboke anticline (or anticlinolium). The axis of the Yakushi anticline plunges 0°～10° to the west. The hinge line or the fold axis is considered as almost rectilinear from its trace on the geological map (Fig. 2) from Sagano in the east to Akaboshiyama in the west of the district. The axial plane is nearly vertical in the east part near Sagano,

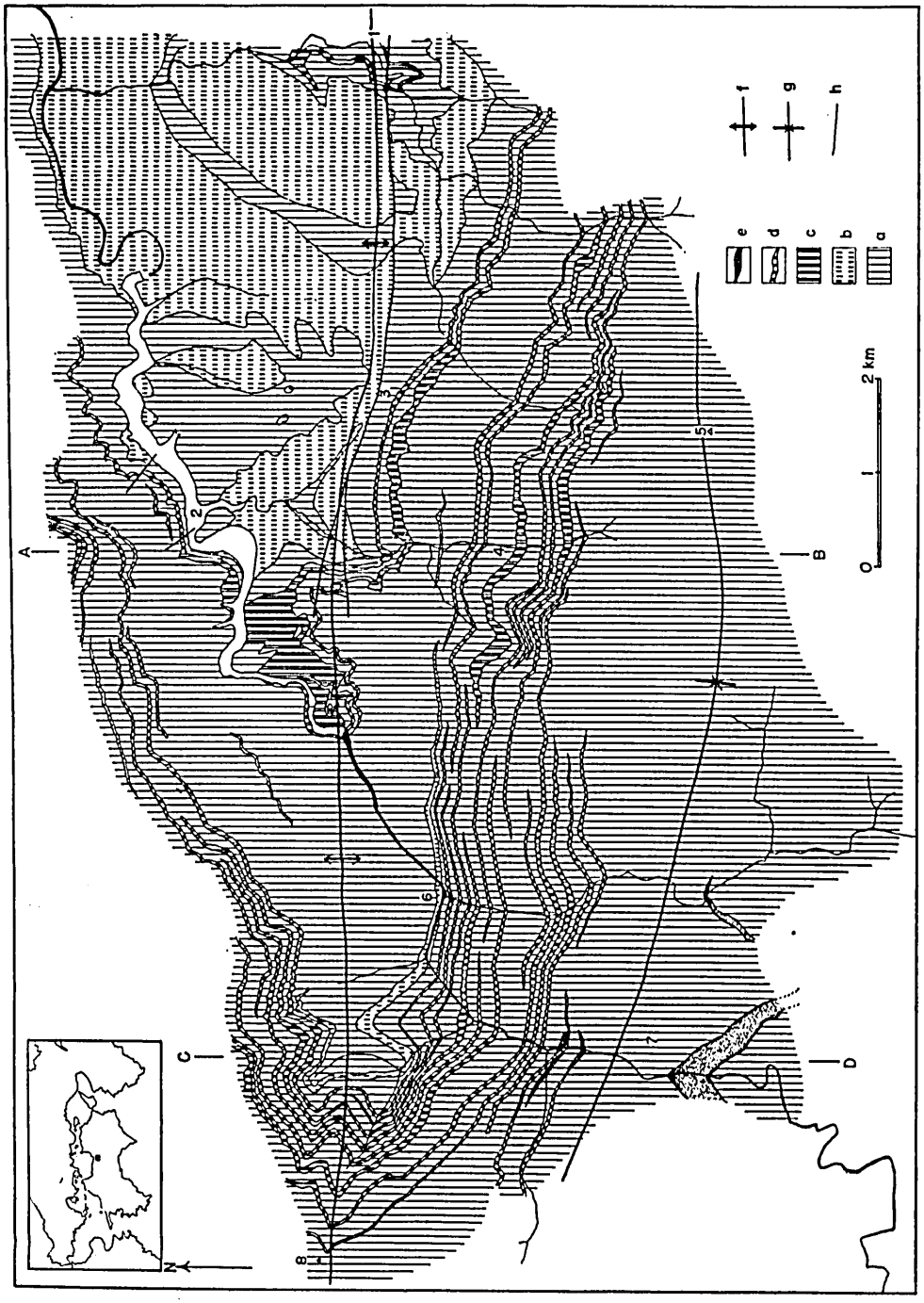
h
g
f
e
d
c
b
a
2 km
0
1
A
B
C
D
N

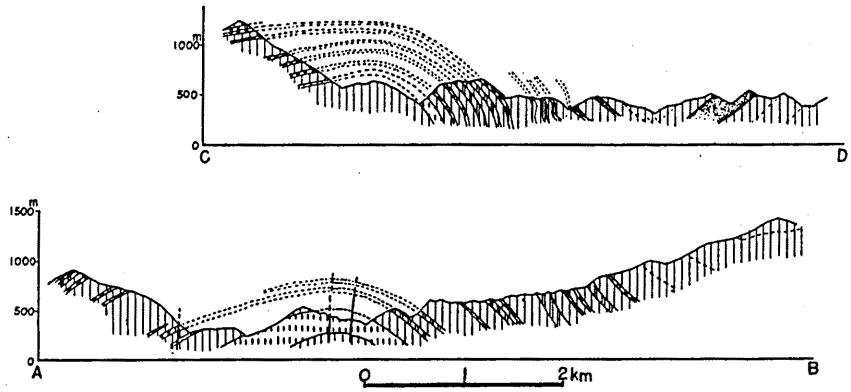

FIG. 2 Geological map of the Sazare Mining District.
a : Pelitic schists b : Psammitic schists c : Basic schists d : Silliceons schists
e : Ultra-basic rocks f : Axial trace of the Yakushi anticline g : Axial trace of the Tsuneyama syncline h : Fault
1 : Sagano 2 : Ogawabashi 3 : Yakushitôge 4 : Sazare Mine 5 : Sazaraeoyama
6 : Tomisatobashi 7 : Fujiwara 8 : Akaboshiyama

Yakushitoge, and Kamiogawa and the fold has an orthorhombic symmetry (C_{2v}). The axial plane dips northwards in the west part near Tomisato and the fold has a monoclinic symmetry (C_{1h}). Therefore, when seen on a large scale, the fold may belong geometrically to non-plane non-cylindrical one in the sense of TURNER and WEISS (1963), having a triclinic symmetry (C_1).

The Tsuneyama syncline is situated to the south of the Yakushi anticline. The axial trend varies from E-W in the area near Sazareoyama to NW-SE in the area between Fujiwara and Nakao, and is not rectilinear. In the west of the region, the axial surface of the syncline is probaly vertical, as judged from small scale folds developed in the axial zone. Therefore, the syncline may be called non-plane non-cylindrical. The small scale folds show somewhat similar style in the axial zone. The horizontal distance between the Yakushi anticline and the Tsuneyama syncline is 3km to 4km. Dip of the limb of these folds is variable. It is symmetrical with respect to the axial plane in the area near the Kamiogawa, but asymmetrical in the area near Fujiwara. In the latter area southern limb of the anticline (northern limb of the syncline) is vertical or overturned, while the northern limb of the anticline dips gently.

On the southern limb of the anticline, a fold of complicated style is observed in the Sazare mine. It was discovered in the progress of ore prospecting by geologists of the mine (DOI, 1959; HIRATA, 1959) and named the Tomisato fold. The axis of the fold plunges 55° to S40°W. Therefore, it is discordant with the regional trend of large scale fold axis. The style of the fold is concentric and imperfectly conjugate. The fold has a conical form along the fold axis. Lacking symmetry plane, the fold has triclinic symmetry (C_1).

2. *Faults*

Large scale faults were shown on geological maps so far published along the axis of the anticline and the syncline (SATO, 1938; KOJIMA, 1951; TAKEDA, 1954; DOI, 1959). The Yakushi-fault along the axial zone of the Yakushi anticline can be recognized in the east of the region, but not to the west of the Kamiogawa by present author. Evidence of the Tsuneyama fault along the axial zone of the Tsuneyama syncline can not be observed.

D. COMPONENT ROCKS

1. *Crystalline schists*

Crystalline schists in this districts are composed of pelitic, psammitic, basic, and siliceous schists. Pelitic schists are considered to be derived from pelitic rocks from their black colour and mineral composition. They show distinct alternation of white and black layers. Psammitic schists show gryish colour and distinct schistosity. They are considered to be derived from psammitic rocks because many clastic minerals are detected in these schists. Basic schists show light to dark green colour. Development of schistosity is variable in basic schists. The original rocks are probably basic tuff and lava. NAKAYAMA (1960) considered that some of them have been derived from intrusive rocks. Siliceous schists are composed mainly of quartz and show distinct schistosity. Their colour are various from light green, brown, dark red, and black, according to accessary minerals. The original rocks of siliceous schists are considered to be chert. In the Ojoin formation, thin layers of calcareous schists which are composed mainly of calcite are included.

2. *Ultra-basic rocks.*

Ultra-basic rocks occur in crystalline schists in the axial zone and the limb of the Tsuneyama syncline. The contact surface between ultra-basic rocks and crystalline schists are parallel to the schistosity surfaces of crystalline schists, and some types of folds and lineations are common in both rocks. Within ultra-basic rocks at Fujiwara the following mineral assemblages are recognized:

a) Olivine-serpentine-chlorite-opaque mineral. Grain size of olivine is 1～2 mm. Serpentine cuts across olivine grains. Serpentine has optically negative character, and rectangular shape. Chlorite is optically positive and has higher retardation.

b) Monoclinic pyroxene-garnet-chlorite. This type of rock occurs as veinlets in other ultra-basic rocks. Pyroxene is colourless and $c \wedge Z$ is 39°. Clorite is optically positive.

c) Monoclinic pyroxene-colourless amphibole-zoisite-chlorite-plagioclase. This type of rock occurs relatively as a large mass in rocks of type a. Pyroxene is colourless and $c \wedge Z$ is 39°. Colourless amphibole occurs around the rim of monoclinic pyroxene or independently. In amphibole, $c \wedge Z$ is 16° and $b = Y$. Chlorite is optically positive.

d) Talc-serpentine. Some parts of ultra-basic rocks are composed mainly of talc and serpentine.

3. *Dyke rocks*

This rock cuts crystalline schists but sometimes is parallel to the schistosity surfaces of crystalline schists. The rock shows dark colour and porphyritic texure. Component minerals are quartz (phenocrysts), sodic plasioclase (phenocrysts) and the matrix is glassy.

E. Ore Bodies

In the Sazare district, bedded cupriferous sulfide ore deposits (kieslager) occur in basic schists. The Sazare deposit is situated stratigraphically in the Upper member of the Minawa formation, and consists of six ore bodies (Fig. 19); Kinritsu-, Kongo-, Sazare-, Kinsen-, Kinsha-, and Shimpi-ore bodies (Oda, 1962). These ore bodies are arranged on three horizons, that is, Sazare, Kinritsu-Kongo-Kinsen, and Kinsha-Shimpi horizon (Oda, 1962). The ore shoot is regular with respect to azimuth and plunge and parallel to those of isoclinal folds or lineations with steep plunge (Takeda, 1954; Horikoshi, 1958; Doi, 1959; Hirata, 1959). Isoclinal folds are also observed in the ore bodies. Component minerals of ore bodies are chiefly pyrite and small amount of chalcopyrite, bornite, magnetite, and hematite. In some layers, white mica, chlorite, rutile and tourmaline are found.

III. Mineralogical Zoning

Mineralogical zoning of the Sambagawa crystalline schists was established in the Kanto mountains by Seki (1958) for the first time, while in Shikoku was done by Banno (1959) in the Besshi district and by Hide (1961) in the Besshi-Shirataki district. In the Sazare district, crystalline schists can be divided into four zones, I, IIa, IIb, and III with respect to component metamorphic minerals.

Zone I. To this zone belong the Lower member and the Middle member of the Minawa formation. In basic schists, quartz, albite, calcite, sericite, stilpnomelane, epidote, actinolite, and glaucophanic amphibole can be found usually as constituent metamorphic minerals. This zone is characterized by stable presence of actinolite. Grain size of these minerals in this zone is smaller than those in the zones II and III. As accessary minerals, leucoxene, sphene, tourmaline and opaque minerals are found. Quartz and albite are small in amount. Two types of chlorites, optically positive and negative, can be observed. Optically positive chlorite is larger in amount than negative one. Sericite is relatively rare. Stilpnomelane concentrates usually in some layers and often develops radially. Stilpnomelane-rich layers in basic schists show often boudinage structure. Epidote in a small rounded ellipsoidal form and showing pleochroism from colourless (X and Y) to yellow (Z) is found commonly in the basic schists in this zone. Actinolite is colourless to very pale bluishgreen (Z) and shows an acicular or fibrous form, having parallel or random orientation with respect to its longest dimension. In this minerals, $b=\mathrm{Y}$, $c\wedge\mathrm{Z}=18^\circ$ and $2\mathrm{V}_x=58^\circ\pm4^\circ$. The value of $2\mathrm{V}_x$ is smaller than that of normal actinolite and rather approximates to that of

1. Basic schists

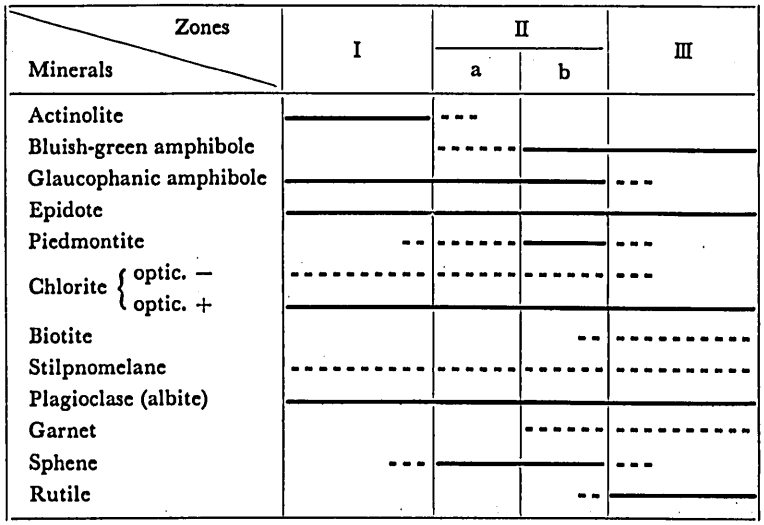

2. Pelitic and psammitic schists

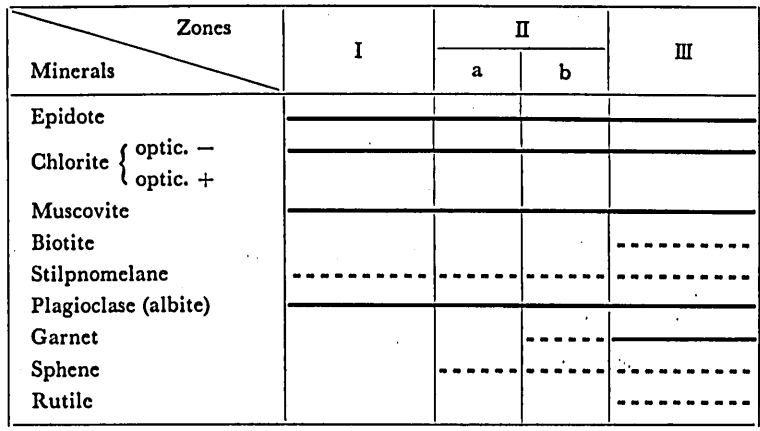

Fig. 3 Stability ranges of metamorphic minerals in the Sambagawa crystalline schists in the Sazare district.
A full line shows that the mineral concerned is common. A broken line shows that it is rare.

glaucophanic actinolite reported by Iwasaki (1963). Alkali-amphibole is often found to form the core of zoned crystal of amphibole. These zoned crystals are usually larger in grain size than crystals of actinolite. Border of the zoned crystal is colourless or pale-coloured actinolitic amphibole. Alkali-amphibole has the following optic properties: $b=Z$, $c\wedge Y=27°$, $2V_x=45°\sim70°$, Z=pale violet~pale-bluish-violet, Y=pale-blue and X=colourless to pale-yellow. The mineral is considered to belong to subglaucophane (crossite) or magnesioriebeckite (Miyashiro, 1957; Miyashiro and Banno, 1958).

In siliceous schists, quartz, albite, chlorite, sericite, stilpnomelane, and epidote are found as constituent minerals.

In pelitic and psammitic schists, quartz, albite, calcite, chlorite, sericite and stilpnomelane are found as metamorphic minerals. As accessary minerals, graphite, epidote, allanite, tourmaline and apatite are found. Chlorite with optically negative character is found, while positive type is rare. The zone I in this district can be considered to be correlated to the zone Ib in the Besshi-Shirataki district after HIDE (1961), or to the lower part of the zone Ib after BANNO (1959) in the Besshi district.

Zone II. In this zone, pale-coloured actinolite is not stable but bluish-green actinolite or bluish-green hornblende are stable. Albite crystals are observed generally as prophyroblasts in this zone. Grain size of minerals in this zone is generally larger than that in the zone I. This zone is subdivided into two subzones, IIa and IIb. The zone IIb may be correlated to the zone II in the Besshi-Shirataki district (HIDE, 1961) or in the Besshi district (BANNO, 1959).

Subzone IIa. To this subzone belongs the lower part of the upper member of the Minawa formation. In basic schists, quartz, albite, calcite, sericite, stilpnomelane, epidote, bluish-green actinolite, and alkali-amphibole can be found usually as metamorphic minerals. Bluish-green actinolite shows pleochroism with X = colourless, Y = pale-green and Z = pale-bluish-green and $b = Y$, $c \wedge Z = 16° \sim 18°$ and $2V_x = 66° \sim 76°$. $2V_x$ of the mineral approximates to that of glaucophanic actinolite (IWASAKI, 1963). Alkali-amphibole has optical properties of $b = Z$, $c \wedge Y = 8° \sim 9°$ and $2V_x = 40° \sim 45°$ and shows pleochroism with X = colourless to pale-yellow, Y = pale-blue and Z = pale-violet. Optic angle of epidote is 74° to 86° (over X, $b = Y$). Epidote shows pleochroism with X = Y = colourless and Z = yellow. In zones II and III; albite grains are found generally as porphyroblasts. Grain size of porphyroblastic albite is small in zone IIa. As accessary minerals, sphene, tourmaline, apatite and opaque minerals are recognized.

In siliceous schists, piedmontite is found as small rounded prismatic crystals. In pelitic schists and psammitic schists, quartz, albite (porphyroblast), calcite, chlorite, sericite, stilpnomelane, epidote, graphite and sphene are usually observed as metamorphic minerals. Chlorite is optically negative.

Subzone IIb. To this subzone belong the Upper member of the Minawa formation and the lower part of the Ojoin formation. In basic schists, quartz, albite, calcite, chlorite, muscovite, stilpnomelane, (biotite), epidote, bluish-green hornblende and glaucophanic amphiboles can be found usually as metamorphic minerals. In siliceous schists, quartz, albite, calcite, epidote, piedmontite, chlorite, muscovite, biotite, bluish-green hornblende, colourless amphibole are usually found. As accessory minerals, garnet, sphene, rutile, hematite, pyrite and chalcopyrite can be observed. Grain size of these minerals in this zone are generally large.

This zone is characterized by the presence of bluish-green hornblende (including barroisite; IWASAKI, 1960). Glaucophanic amphiboles occur as isolated grains or as

the rim of bluish-green hornblende. The core of some amphibole crystals is glaucophanic amphibole and the rim is bluish-green amphibole. Bluish-green amphibole shows following optic properties: $b = Y$, $c \wedge Z = 19° \sim 23°$ and pleochroism with X = colourless to pale-yellow, Y = pale-green to green and Z = pale-bluish-green to bluish-green. $2V_x$ varies from 36° to 76°. Some of these bluish-green amphibole may belong to barroisitic hornblende (Iwasaki, 1960b, 1963). Relatively dark bluish-green amphiboles have smaller optic angles than pale-coloured one. One of bluish-green amphibole from Sarutagawa is $b = Z$, $c \wedge Y = 23° \sim 25°$ and $2V_x = 21° \sim 24°$. In piedmontite-bearing siliceous schist at the 6th sublevel of the Sazare Mine, almost colourless glaucophane is found and its optic properties are as follows: $b = Y$, $c \wedge Z = 20°$, $2V_x = 65°$, with weak pleochroism of $X = Y$ = colourless and Z = colourless to very pale-blue. Other types of glaucophanic amphiboles show $b = Z$ and $2V_x = 62° \sim 75°$. Pleochroic colours are X = colourless to very pale-yellow, Y = pale-blue, and Z = violet. Chlorite of optically positive type is usually found, but that of negative type is rarely recognized in some layers rich in garnet. Biotite with brown colour (X = colourless and Y = Z = lightbrown) is found with chlorite (optically positive), muscovite, stilpnomelane, albite, quartz and calcite at the 18th level of the Sazare mine. Albite porphyroblasts (An 0~8) include often small grains of quartz, calcite, epidote, amphibole, sphene, rutile and opaque minerals. Piedmontite often shows zoning. In this case, the core of the zoned crystal is piedmontite and the rim is pistacite-clinozoisite. Pleochroic colour of piedmontite is X = light yellow, Y = pink and Z = red.

In pelitic schists, main constituent minerals are quartz, albite (porphyroblast), chlorite, muscovite, stilpnomelane, garnet and accessory minerals are graphite, sphene, and tourmaline. Chlorite is optically negative.

Zone III. To this zone belongs the Ojoin formation except the lower part. This zone is characterized by the presence of biotite in pelitic schists. In pelitic schists, quartz, albite (porphyroblast), garnet, chlorite, muscovite and biotite are usually found as main component minerals and sphene, rutile and tourmaline are often found as accessary minerals. Biotite is small in grain size (0.04~0.2 mm) and shows pleochroism with X = brownish-yellow and Y = Z = brown. Chlorite is optically negative. Garnet and albite occur as porphyroblasts.

This zone may be correlated to the zones IIIa and IIIb after Hide (1961) in the Besshi-Shirataki district, or the higher part of the zone II to the lower part of the zone III after Banno (1959) in the Besshi district. The zone IV in the Besshi-Shirataki district (Hide, 1961) can not be found in the Sazare district.

As described in the preceding pages, the boundary lines between these zones are nearly parallel to the stratigraphical ones except in the western area near Fujiwara. General tendency that metamorphic grade of the stratigraphically higher levels is higher than that of the lower levels in Central Shikoku can also be recognized in this district.

IV. Mesoscopic Analysis

The chief objects in mesoscopic analysis of rock structure in this chapter are to describe characteristic styles of rock structures, and to clarify mutual relations between those structures. As conspicuous rock structures will be treated planar structures, linear structures and folds on small scales.

A. Planar Structures

The most predominant and principal schistosity surface has been termed S_1 in the Sambagawa crystalline schists of Central Shikoku by Kojima and Suzuki (1958) and Kojima and Hide (1958). The surface S_1 is parallel to the compositional banding or the lithologic layering of the crystalline schists on all scales. From this point, the surface S_1 might be derived from original bedding surface, although clear remnants of sedimentary structures have not been observed in this district. In many cases, metamorphic minerals show planar preferred orientation of grain boundaries parallel to the surface S_1. {001} in micas and chlorites and {100} in amphiboles are generally parallel to the surface S_1.

In the Sazare district, S_1 is defined by lithologic layering probably derived from original bedding and dimensional orientation of minerals, that being consistent with the general nomenclature in the Sambagawa metamorphic zone.

In the domains where isoclinal folds are developed, however, lithologic layers on a small scale show fold-forms and in the hinge zone are oblique to the preferred dimensional orientation of minerals which is parallel to the axial surface of fold (Fig. 4a). In this paper, the following symbols are used as defined by Hide (1961).

s_1 : the lithologic layering or compositional banding on a small scale;
s_2 : the axial surface of small-scale isoclinal folds;
s_m : the preferred dimensional orientation of metamorphic minerals.

The cleavage surface with chracteristics of strain-slip cleavage or of fracture cleavage in the sense of Leith (1905), de Sitter (1956), Knill (1960), and Turner and Weiss (1963) is developed in the Sambagawa crystalline schists. This type of S-surfaces has been termed S_2 and S_3 by Kojima and Suzuki (1958). This type of cleavage cuts across S_1 at variable angles and shows often weak transposition of preexisting foliation S_1. Finely laminated micaceous layers (S_1) are often folded and transposed to S_2 near walls of a microlithon, a domain enclosed between two surfaces of S_2. Spacing of S_2 is about 0.1～2 cm. In rocks composed by alternation of pelitic schists and psammitic schists, S_2 develops well in pelitic schists but less develops or lacks in psammitic schists-layers. This relation of competent and less competent layers can be recognized in such rock associations as psammitic schists-pelitic schists, calcareous schists-pelitic schists, and basic schists-pelitic schists. S_2 is parallel or almost parallel to axial surfaces of small-scale folds of concentric similar style (see page 16). In this case, S_2 is generally normal to or oblique to the enveloping surface of folds. Two types of S_2-surface can be recognized.

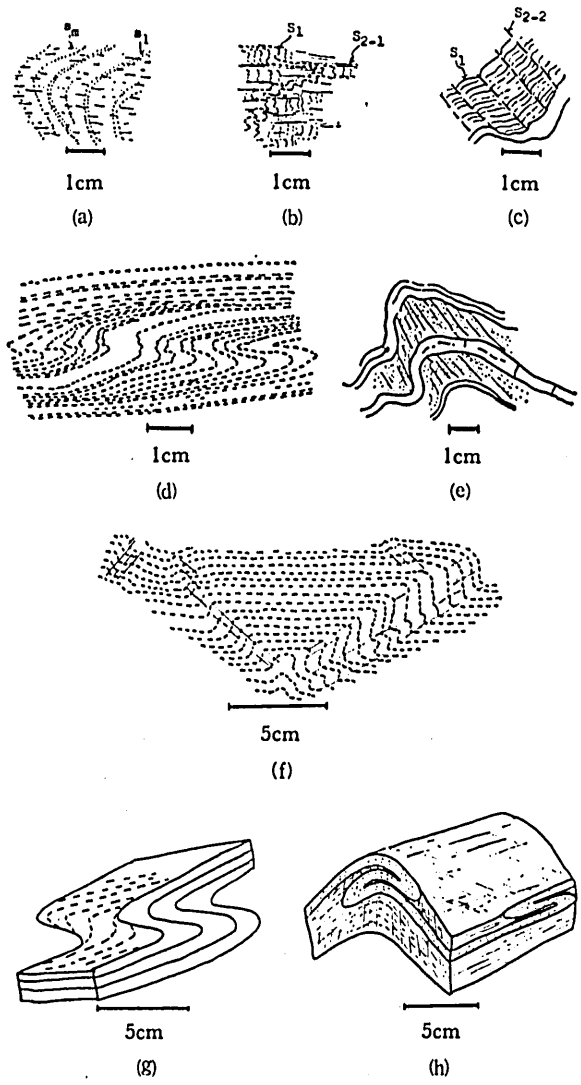

Fig. 4 Sketches of small scale folds and schistosity surfaces.
a : Relation between s_1 and s_m.
b : Relation between S_1 and S_{2-2}.
c : Relation between S_1 and S_{2-2}.
d : Style of the type I fold.
e : Style of the type III fold.
f : Style of the type IV fold.
g : Relation between L_m and the type II fold.
h : Relation between the type II and the type III fold.

S_{2-1}: This surface is characterized by the intense transposition of S_1 by the cleavage. The surface of preferred orientation of basal cleavage in mica is rotated to this surfaces (Fig. 4b). In the hinge zone of folds on a microscale, the orientation

of basal cleavage in mica is not controled by the axial surface of the folds but controled by S_1 as shown in Fig. 27b, and micas are often polygonal.

S_{2-2}: In this surface, transposition of S_1 by this surface is weakly recognized (Fig. 4c). In the hinge zone of the associated folds on a small scale (type III and type IV folds which will be described in page 16), micas and chlorites are usually bent as shown in Fig. 27c.

In some places, it is observed that S_{2-1}-surfaces are crossed and folded by S_{2-2}-surfaces. From these observations, S_{2-1} must be earlier than S_{2-2}. In the axial zone of the Tsuneyama syncline, S_{2-2} is nearly vertical. In the zone of the Yakushi anticline, conjugate sets of S_{2-1} or S_{2-2} can be observed, in general symmetrically oblique to S_1.

B. Linear Structures

L_1. L_1 is the lineation defined by the intersection of s_1 and s_2. It is observed as very fine streaks on S_1. The intersection is parallel to the axis of an isoclinal fold on a small scale.

L_m. L_m is the lineation defined by preferred orientation of the longest dimension of prismatic minerals such as amphiboles, epidote and tourmaline. This lineation is generally parallel to L_1.

L_2. L_2 is the lineation defined by the intersection of S_1 and S_{2-1}. This lineation is observed as fine streaks.

L_3. L_3 is defined by the intersection of S_1 and S_{2-2}. This lineation is observed as microcorrugations on S_1 or as microcrenulations.

L_4. L_4 is the lineation defined by the intersection of S_{2-1} and S_{2-2}. This lineation is observed also as microcorrugation on S_{2-1}.

C. Folds

1. *Style of small-scale folds*

Type I. Isoclinal folds, "isoclinal" similar folds and/or intrafolial folds are observed in crystalline schists in this district. In these folds, some layers are thick in the hinge zone but are often thinning out towards the limbs of the folds. Therefore, they are often rootless folds. These folds are called type I folds in this paper. Profiles of this type of folds are shown in Fig. 4d and Fig. 2 in Plate 30. The axial surface of the type I folds is parallel to S_1 which is recognized as gross lithologic layering as shown in Fig. 4d. The amplitude of the fold is much larger than the wave-length. Geometrically, the type I folds is plane cylindrical, but sometimes plane non-cylindrical. The symmetry of the type I folds is monoclinic (C_{1h}).

Many small-scale folds of type I are observed in siliceous, basic, and pelitic schists, rarely in psammitic and calcareous schists. The occurrence of the type I folds is not restricted to any zone of metamorphic grade. Where this type of folds are developed, S_1 shows undulating surface and the axis of waves is parallel to the isoclinal fold axis. Rodding-like part or elongated vein of quartz and plagioclase can be observed.

Their long axes are generally parallel to the fold axis. Although the relation between the type I folds and preferred orientation of metamorphic minerals is described in page 0, the results indicate that the *c*-axis of amphiboles and the *b*-axis of epidotes are parallel to the axis of the type I fold, and {001} in mica is parallel to the axial surface of the fold (page 27). The axis of the type I fold is termed B_1 in this paper. The lineations related to B_1 are L_1 and L_m.

Type II. This type of folds shows styles of similar folds, being accompanied by cleavage surfaces S_{2-1}. It is observed in pelitic schist intercalated with thin layers of psammitic schist in fine grained psammitic schist and in basic schist. Fig. 1 in Plate 29 shows one of examples of the type II folds. The ratio of amplitude/wavelength (A/W-ratio) is 1.5～1.7. Axial surface of the fold is nearly parallel to or oblique to S_1 at small angles. The symmetry of this type of folds is monoclinic (C_{1h}). Under the microscope, mica plates surrounding the hinge zone rarely show bending but are often polygonal (page 29). The axis of the type II folds is termed B_2 in this paper. The related lineation to B_2 is L_2.

Type III. This type of folds is defined by combination of concentric or flexure folds in competent layers and cleavage folds in less competent layers, the style resembling similar fold. Profiles of some examples of the type III folds are shown in Fig. 4e and Fig. 2 and 3 in Plate 29. This type of folds, however, can not be considered to be similar folds in the strict sense, because the foldform is not constant along the axial surface as shown in Fig. 2 of Plate 29. Concentric or flexure folds are observed in psammitic calcareous and siliceous schists intercalated in pelitic schists or in basic schists, while cleavage folds are developed in micaceous layers in pelitic schists and in mica-chlorite-rich layers in basic schists. Axial surfaces of the type III folds are normal or oblique to S_1 (generally 30°～90°). The cleavage surfaces accompanying this type of folds belong to S_{2-2}. The fold-form is of an open style and A/W ratio is 0.4 to 1. This value is much smaller than that of the type II fold. Geometrically, the type III fold is generally plane-cylindrical. The symmetry of the fold is orthorhombic (C_{2v}) or monoclinic (C_{1h}). The axis of the type III fold is termed B_3 in this paper. The related lineations to B_3 are L_3 and L_4.

Folds of type III are observed in every horizons of stratigraphic sequence and every zones of metamorphic grade, except in thick psammitic schists beds.

Type IV. The style on the ac-profile of the type IV folds is shown in Fig. 4f. The axial surfaces of a conjugate fold occur in a conjugate set (Fig. 4f). Strain slip cleavages or fracture cleavages occur associated with the folds parallel to the axial surfaces of the fold. These cleavages are identical in nature with those associated with the type III folds, belonging to S_{2-2}. The type IV folds are identical with the type III folds in many characteristics except their conjugate style. The symmetry of the fold is orthorhombic (C_{2v}) or monoclinic (C_{1h}). The axis of the type IV fold is also termed B_3.

Type V. This type of fold is defined by angular bending of S_1 resembling to kink band. Therefore, it is identical with kink fold in the sense of Turner and Weiss

(1963). The type V folds can be observed in well foliated rocks. The axial surface is generally normal to or oblique to S_1. Scale of the folds is generally small in size and wave length is in order of 2 cm to 5 cm. Geometrically, this type of fold is plane cylindrical fold and the symmetry of the fold is generally monoclinic (C_{1h}). The axis of the type V fold is termed B_5.

2. *Orientation of small scale folds*

In the type I folds, plunge of fold axes is very variable, horizontal to vertical, and their azimuth veers from NS to SE. In the lower and middle members of the Minawa formation the azimuth of these folds is E-W to WNW-ESE and parallel to the axis of the large-scale fold, the Yakushi anticline. In the upper member of the Minawa formation to the Ojoin formation, the axes of these folds are preferably orientated in N-S to NE-SW.

The axial surfaces are parallel to or nearly parallel to S_1, but the dip angle of the surface is variable according to that of S_1. It is nearly horizontal near the crest of the Yakushi anticline, and is nearly vertical on the limb of the anticline.

The orientation of axis of the type II folds is also variable, and the dip of the axial surface varies according to the change in dip of S_1.

The axes of the type III and IV folds are almost constant in orientation, horizontal to slightly plunging (Fig. 7b).

3. *Mutual time relations of folds*

In spotted basic schist 1 km north of Fujiwara, superposed structures between L_m and the type II folds are observed. The lineation L_m which is characterized by preferred orientation of c-axes of amphibole and b-axes of epidote was bent or folded around the hinge of the type II folds. Therefore, it can be inferred that L_m is earlier than the type II folds.

In spotted pelitic schist at Fujiwara, a fold similar to the type II folds was superposed with the type III folds. Fig. 4h shows one of their examples. Fold axes, axial surfaces and lineation L_2 are crossed obliquely and curved around the fold axis of the type III fold. Cleavage surfaces parallel to the axial plane of the type III fold is strain-slip cleavage S_{2-2}. Projection of L_2 lies neither on a small circle with the centre coinciding with the fold axis of the type III fold, nor on single great circle (as discussed by WEISS (1959) and by RAMSAY (1960)). Therefore, type III fold can be regarded neither as a flexural slip fold nor a shear fold.

In spotted pelitic schist 1 km north of Fujiwara, it is observed that the type II folds were superposed by the type III folds. Although development of the type III folds is weak, axial surfaces of the type II folds and S_{2-1} are intersected by S_{2-2} which accompanied the type III folds. Therefore, the type II folds are concluded to be older than the type III fold. Basal cleavages of mica which are parallel to S_{2-1} are observed under the microscope to have been bent around the type III folds or cut by S_{2-2}. This texture is observed in pelitic schists of the zone I north of the Sazare mine. At Sagano north-east of the Sazare mine, mutual relation of three types of

folds and *s*-surfaces can be clearly recognized in pelitic schist of the zone I. The type I folds on a small scale were folded around the type II folds. The type II folds and associating surface S_{2-1} were again folded around the type III folds with axial cleavage S_{2-2}.

The type V folds refold or bend folds of other types as well as lineations L_1, L_m, L_2, and L_3, and surfaces S_{2-1}, and S_{2-2}. Therefore, the type V folds were formed later than other types of folds and accompanying lineations and *s*-surfaces.

From these observations, it can safely be concluded as follows: The type I folds are the earliest structures; then the type II folds, S_{2-1} and L_2 were formed; the type III and IV folds, S_{2-2}, L_3 and L_4 are younger than the type II folds, S_{2-1} and L_2; and the type V folds are the latest of the folds in this district.

4. *The Tomisato fold.*

The Tomisato fold is a down-dip fold in spotted basic schists discovered by geologists of the Sazare mine (Hirata, 1959 and Doi, 1959) at the Tomisatomuke prospecting gallery (at the 12th level). In the horizon of ore bodies of the Sazare mine axes of various types of folds including the Tomisato fold and associated lineation plunge steeply to SW. The style of the Tomisato fold on the horizontal section shows a unique form as shown in Fig. 5 and seems to belong to the type II folds. The west hinge of the Tomisato fold is sharp in form. The east hinge is rounded. The axial surface of the west hinge strikes E-W and dips steeply southward, while that of the east hinge strikes NW-SE and dips steeply southward. Change of style along the fold axis can not determined directly because no galleries have been cut across the Tomisato fold at levels other than the 12th level. However it is inferred

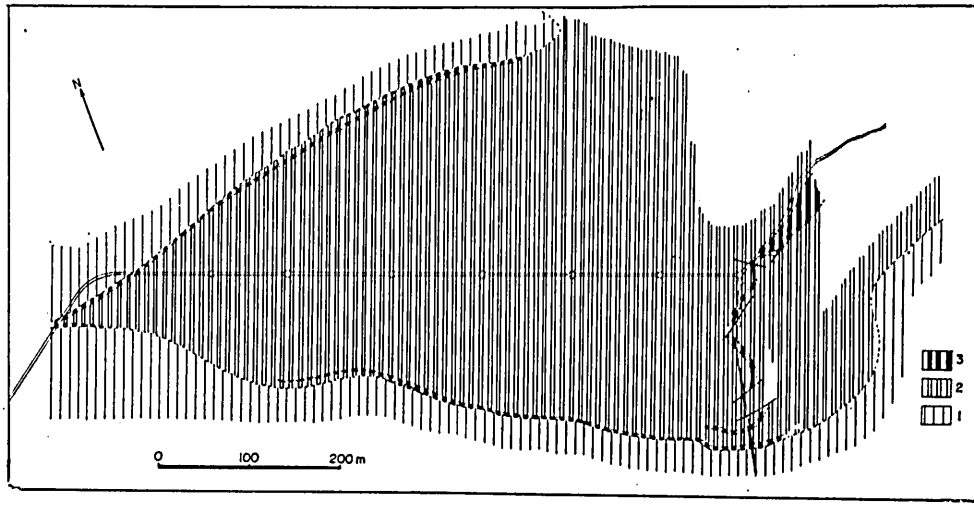

Fig. 5 Underground geological map of horizontal section including the Tomisatomuke prospecting gallery at the 12th level, after the Sazare Mine (1961), and partially revised by the present author.
1 : spotted pelitic schist. 2 : spotted basic schist. 3 : spotted siliceous schist.

from macroscopic analysis (see page 302) to be a conical form. Therefore, the symmetry of the fold with respect to its geometric elements and folded surface is triclinic (C_1).

Small-scale folds observed in the Tomisatomuke prospecting gallery are various in type. Small-scale isoclinal folds which belong to the type I folds as described in the preceding pages are recognized. The fold axis of this type I fold (B_1) plunges steeply (40°～90°) and its azimuth is generally SW. The axial surface is parallel or nearly parallel to S_1 and both surfaces dip 50°～90° to the south. Although the type II folds are recognized at many places in the gallery, but they are developed especially well in both hinge zones of the Tomisato fold. In this fold, epidote-rich layers show generally concentric or flexure folds, while in mica- and chlorite-rich layers strain-slip cleavages are developed. The fold form is plane cylindrical. The axial plane is oblique to S_1. The symmetry of the folds with respect to geometric elements and folded surface is monoclinic (C_{1h}). In the west hinge, fold axes of the type II folds (B_2) plunge steeply southward and are parallel to or almost parallel to those of the type I folds (B_1). In the west part of the gallery, axial surfaces of the type II folds strike almost E-W and parallel to that of the Tomisato fold. In the east hinge axes of the type II folds (B_2) plunge moderately or steeply (30°～80°) southwestward. The strike of axial surfaces of the type II folds is variable in the east hinge.

Folds of the types I and II were refolded by later folds of the type III. This relation is also recognized in linear structures. Lineation L_1, L_m, and L_2 are intersected by later developed horizontal lineation L_3, the intersection of S_1 and S_{2-2}, associated with the later formed type III folds.

In the domain of the Tomisato fold, no difference in the orientation of fold axis has not been recognized between the type I and the type II folds.

V. Macroscopic Analysis

A. Macroscopic Analysis of the Yakushi Anticline and the Tsuneyama Syncline

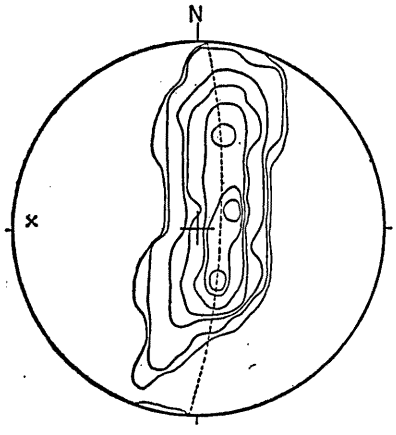

Fig. 6 S_1-pole diagram of the total domain of the Sazare Mining district. A broken line represents π-circle for S_1 and a cross represents β_{51}. 1174 points. Contours: 9-7-5-3-2-1-0.5%.

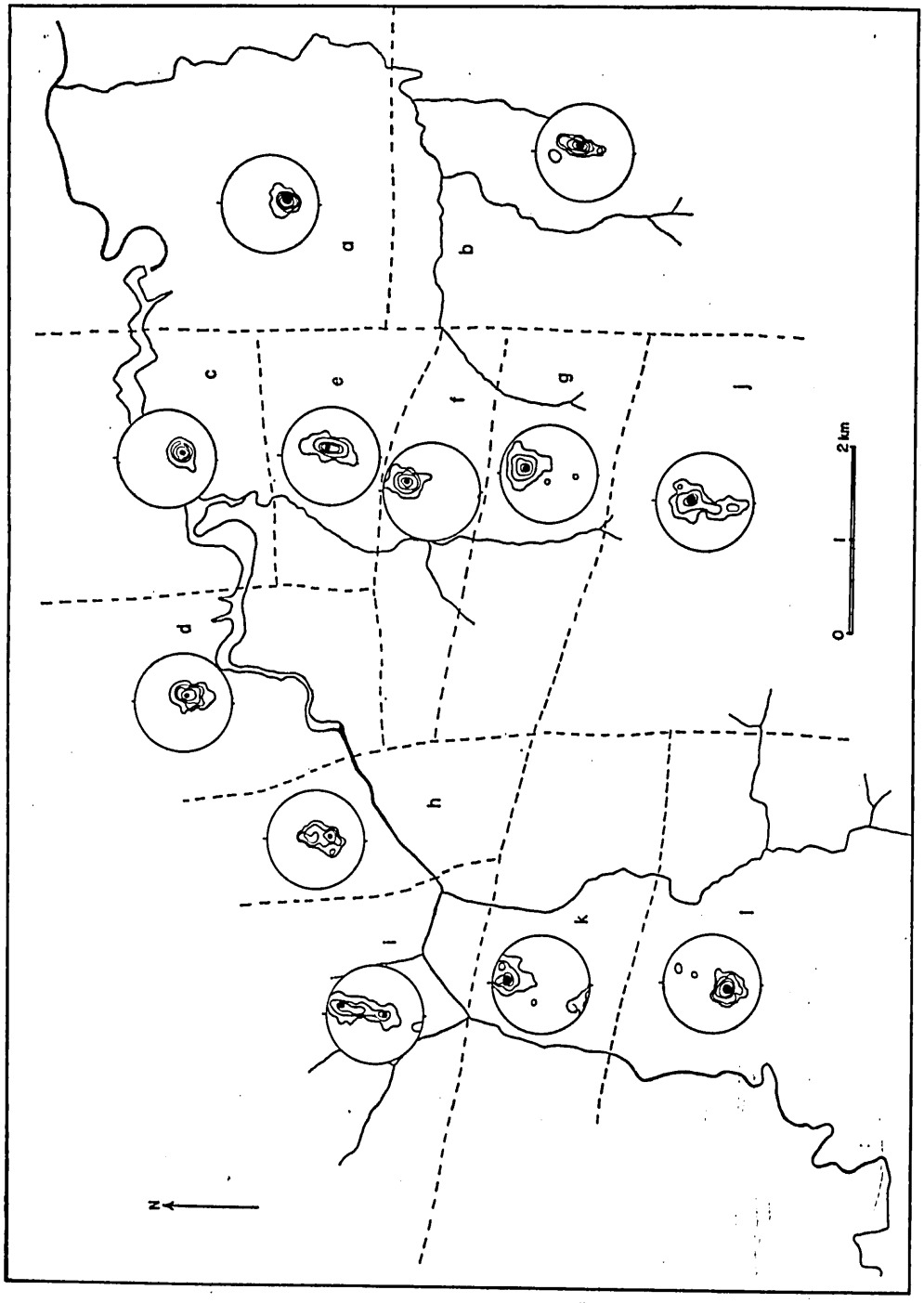

Fig. 7a S_1-pole diagrams in tentatively divided subareas. Contours: 30-20-10-5-1%.

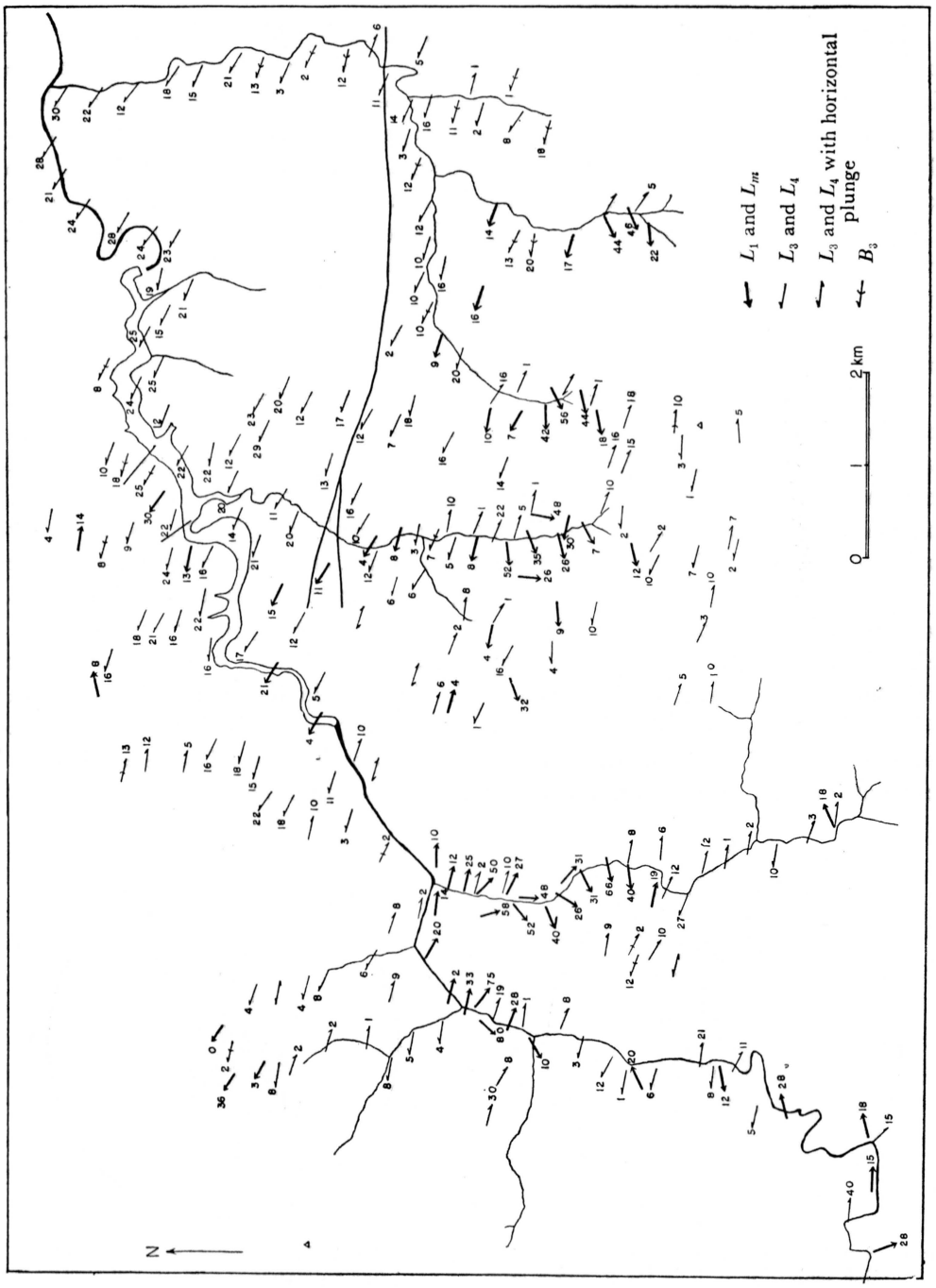

FIG. 7b Lineation map of the Sazare Mining District.

1. *Planar structures*

a. Macroscopic analysis of S_1.

Fig. 6 shows S-pole diagram for S_1 in the total domain which covers the area from the Yakushi anticline to the Tsuneyama syncline. Poles of S_1 fall on a distinct great circle girdle which is π-circle (S-pole circle) for S_1. The pole of the π-circle determins β_{S_1} (β-axis for S_1). The axis β_{S_1} plunges gently to the west (azimuth N87°W, plunge 10°). In the third quadrant of the diagram (Fig. 6), significant deviation of poles of S_1 from π-circle can be recognized. It suggests that the region can not be simply treated as a homogeneous domain. Therefore, homogeneity of the domain with regard to β_{S_1} must be examined. The domain concerned is subdivided into small subareas which are strictly homogeneous with respect to β_{S_1}. Fig. 7a shows S-pole diagram for S_1 in each small domain. These small subareas can be joined into larger domains I (subareas a to i) and II (subareas j to l) in this region. Each domain is homogeneous with respect to β_{S_1} within deviation range of $\pm 5°$. The domain I includes the Yakushi anticline and the domain II does the Tsuneyama syncline. S-pole diagrams for S_1 in each domain are shown in Fig. 8 and 9. In the domain I, β_{S_1} plunges 10° to N88°W as shown in Fig. 8, coinciding with the axis of the Yakushi anticline, which is shown in the geological map (Fig. 2). Style of form surface of the Yakushi anticline is suggested from pattern of the diagram of S_1-pole. It reflects a gently curved, broad axial zone, the moderately inclined north limb and the steeply inclined south limb. In the domain II, however, β_{S_1} is horizontal with azimuth N70°W–S70°E. Therefore, the axis β_{S_1} in this domain is slightly discordant with that in the domain I. The axis β_{S_1} in the domain II is concordant with the axis of the Tsuneyama syncline as read from the geological map (Fig. 2). The pattern of Fig. 9 may somewhat reflect the mesoscopic type III folds in the axial zone but is consistent with macroscopic style as shown in profiles (Fig. 2).

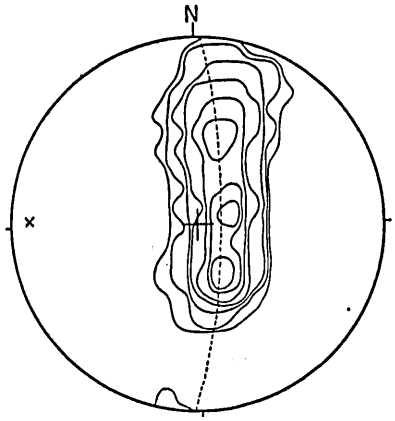

Fig. 8 S_1-pole diagram of the domain I. A broken line represents π-circle for S_1 and a cross represents β_{S_1}. 977 points. Contours: 9-7-5-3-2-1-0.5%.

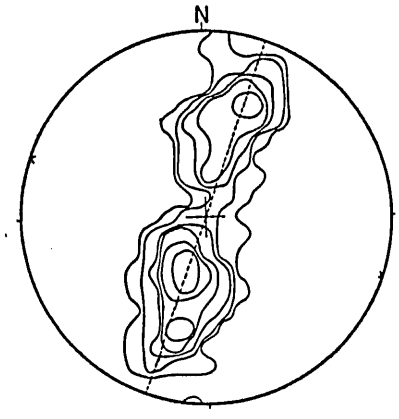

Fig. 9 S_1-pole diagram of the domain II. A broken line represents π-circle for S_1 and a cross represents β_{S_1}. 221 points. Contours: 9-7-5-3-2-1%.

b. Macroscopic analysis of S_2-surfaces.

In the domain I, S_{2-1}-surfaces are recognized 1km north of the Sazare mine. The pattern of S-pole diagram for S_{2-1} is somewhat elongated (Fig. 10). The azimuth of β-axis for S_{2-1} (Fig. 10) is slightly displaced from that of β_{S_1} in the domain I. In the domain I, poles of S_{2-2} fall on a girdle (Fig. 11a). The π-circle determins $\beta_{S_{2-2}}$ (β-axis for S_{2-2}). In this domain, $\beta_{S_{2-2}}$ plunges 12° to N71°W and practically coincides with $\beta_{S_{2-1}}$. The $\beta_{S_{2-2}}$ deviates about 20° from that of β_{S_1} in the same domain I. Therefore, S_{2-2}-surfaces are tautozonal with S_{2-1}-surfaces but are not tautozonal with S_1-surfaces in the domain I. In the domain II, the diagram for S_{2-2} shows a

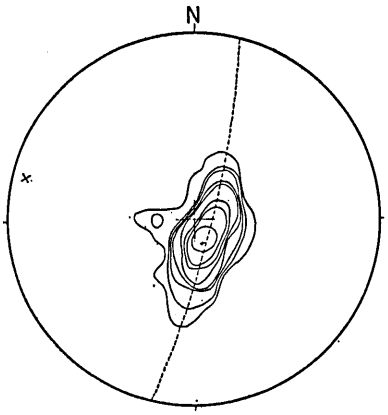

FIG. 10 S_{2-1}-pole diagram on the southwest of Yakushitoge in the domain I. A broken line represents π-circle for S_{2-1} and a cross represents $\beta_{S_{2-1}}$. 107 points. Conturs: 30-24-16-10-6-4-2-1%.

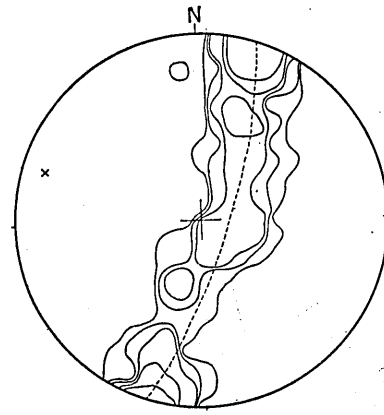

FIG. 11a S_{2-2}-pole diagram of the domain I. A broken line represents π-circle for S_{2-2} and a cross represents $\beta_{S_{2-2}}$. 310 points. Contours: 7-5-3-2-1%.

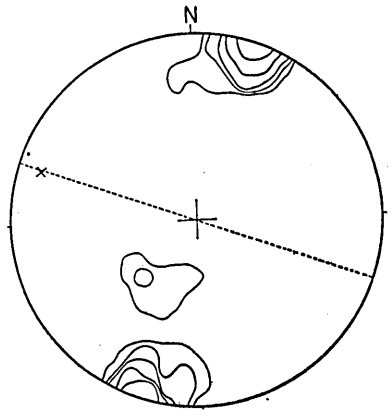

FIG. 11b S_{2-2}-pole diagram of the domain II. A broken line represents the general orientation of S_{2-2}. A cross represents $\beta_{S_{2-2}}$ in the domain I. 43 points. Contours: 20-15-10-5-2-%.

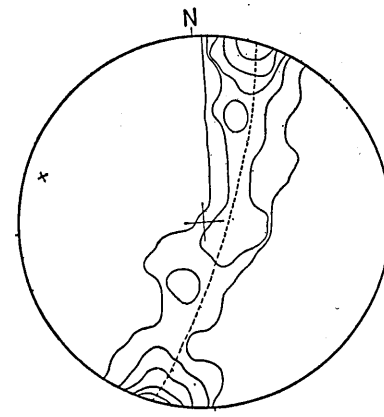

FIG. 11c S_{2-2}-pole diagram of the total domain. A broken line represents π-circle for S_{2-2} and a cross represents $\beta_{S_{2-2}}$. 353 points. Contours: 10-8-5-3-1-%.

maximum which represents general strike N70°W and dip 90° of S_{2-2} (Fig. 11b). This orientation of S_{2-2} in the domain II is concordant with that of $\beta_{S_{2-2}}$ in the domain I, and β_{S_1} in the domain II. Therefore, the domains I and II are co-axial with respect to S_{2-2}. This fact is also expressed in the *S*-pole diagram for S_{2-2} of the total domain which shows a complete girdle with narrow width, as shown in Fig. 11c.

c. Macroscopic analysis of axial surfaces of small-scale folds

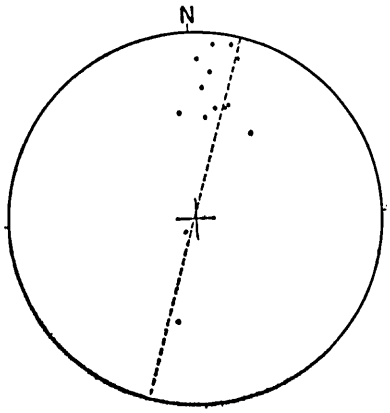

Fig. 12 *S*-pole diagram for axial surfaces of type I folds on the riversides of the Dozan River. Solid circles represent poles of the axial surfaces. A broken line represents π-circle for S_1.

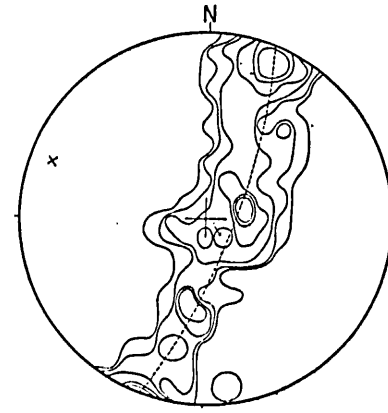

Fig. 13a *s*-pole diagram for axial surfaces of trpe III and IV folds of. the total domain. A broken line represents π-circle for the axial surfaces and a cross represents β-axis for the axial surfaces. 103 points. Contours: 9-7-5-3-2-1%.

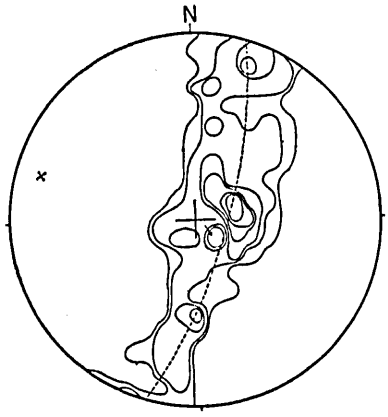

Fig. 13b *s*-pole diagram for axial surfaces of type III and IV folds of the domain I. A broken line represents π-circle for the axial surfaces and a cross represents β-axis for the axial surfaces. Contours: 12-9-7-5-3-1%.

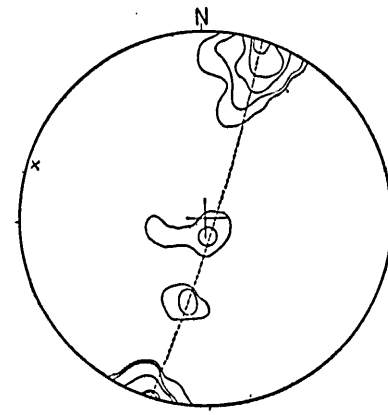

Fig. 13c *s*-pole diagram for axial surface of the type III and IV folds of the domain II. A broken line represents π-circle for the axial surfaces and a cross represents β-axis for the axial surfaces. 43 points. Contours: 27-20-16-8-4%.

Type I folds:—Poles of axial surfaces of the type I folds in the domain II fall on a circle as shown in Fig. 12, poles of which almost coincides with β_{S_1} in the domain II. This macroscopic geometry is consistent with the fact of mesoscopic geometry that axial surface of the type I folds are parallel or nearly parallel to S_1-surfaces.

Type III and type IV folds:—Fig. 13a shows S-pole diagram for axial surfaces of the type III and IV folds in the total domain. A complete girdle is recognized and β-axis for axial surfaces is clearly coincides with $\beta_{S_{2-2}}$ (cf. Fig. 13a with Fig. 11c). In the domains I and II, β-axis for axial surfaces is concordant with $\beta_{S_{2-2}}$ in each domain (cf. Fig. 11a with 13b and Fig. 11b with 13c). The pattern of S-pole diagram for axial surfaces of the type III and IV folds is not different from that of S-pole diagram for S_{2-2}. These relations in macroscopic geometry is consistent with those in mesoscopic geometry.

2. *Linear structures*

a. Macroscopic analysis of L_1

Lineation L_1 and L_m are projected in Fig. 14. The data were measured in the area from the southern limb of the Yakushi anticline to the northern limb of the Tsuneyama syncline and stratigraphically from the upper member of the Minawa formation to the Ojoin formation. A maximum shows that large number of L_1 and L_m plunges moderately to SW-WSW. The pattern of lineation diagram shows that lineations L_1 and L_m are very heterogeneous with respect to their orientation on the scale of the total domain. Heterogeneous patterns of lineations in some domains with complex fold systems have often been clearly analysed by macroscopic analysis of superposed folding (e. g., WEISS and MCINTYRE, 1957). In the mesoscopic analysis (see page 18), the type I folds and associated lineation L_1 and L_m were refolded by the types II, III, and IV folds. It is a problem whether the heterogeneity of L_1 and L_m was due to disturbance by repeated folding or the orientation of B_1, L_1 and L_m was originally heterogeneous before the folding of the types II, III and IV. To examine these questions, a homogeneous domain with respect to L_1 and L_m must be found. Fig. 15a shows lineation diagram for L_1 in the rectangle domain with long

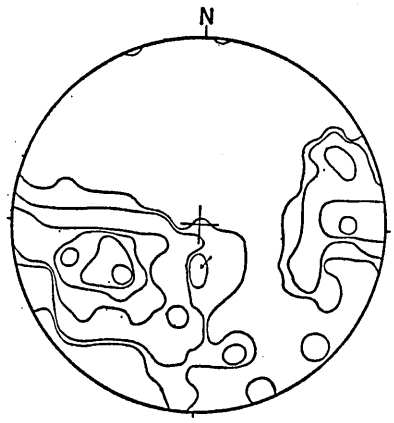

FIG. 14 Lineation diagram for L_1 in the southern part of the domain I and domain II. 190 points. Contours: 10-7-5-3-1-0.5%.

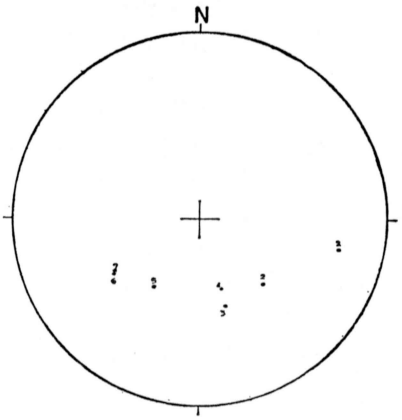

FIG. 15a L_1 in a small area of 230m normal to S_1 and 80m parallel to S_1 from the Saruta River. Solid circles represent L_1 and are numbered aften the horizon of measurement in ascending order. Adimuth and plunge of L_1 changes gradually from the lower horizon (1) to the upper horizon (7).

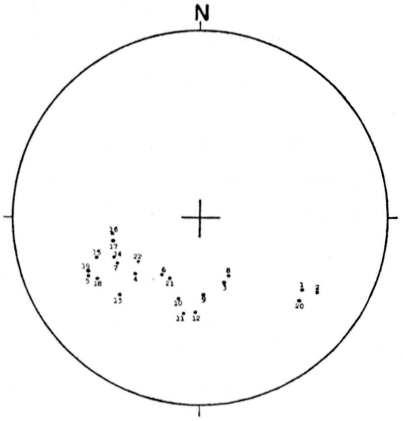

FIG. 15b L_1 in a small area of 750m normal to S_1 and 250m parallel to S_1 from the Saruta River. Solid circles represent L_1 and are numbered after the horizon of measurement in ascending order. L_1 swings in azimuth and plunge from the lower horizon (1) to the upper horizon (22).

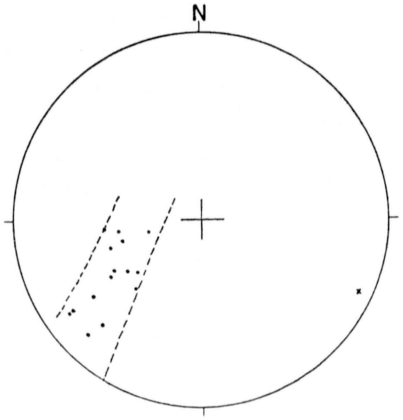

FIG. 15c L_1 in a small area of 150m normal to S_1 and 800m parallel to S_1 from the Shimosaruta. Broken lines show small circles the center (a cross) of which repressents β-axis for S_1 determined by Fig. 15d.

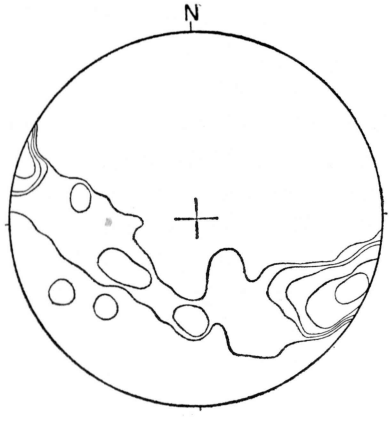

FIG. 15d β-diagram for S_1 in the same area as for Fig. 15c.

edges normal to the strike (230 m) and with short edges along the strike of S_1 (90 m). Plunge of L_1 varies continuously from ESE to SW when one goes from the lower horizon to the upper horizon across the strike of S_1. In another domain, plunge of L_1 swings from SE to SW or vice versa on S_1 from the lower horizon to the upper horizon of the rock sequence, as shown in Fig. 15b. In the latter case, S_1-surface is plane. As any fold axis normal to S_1 can not be observed, the variable or randum orientation of L_1 on S_1-surface can not be attributed to the superposition of folding.

Therefore, it is inferred that the randum orientation of L_1 had been originated before the folding of the type II, III and IV folds. In a small domain of 800 m along and 150 m normal to the strike of S_1, lineation L_1 has relatively regular orientation. In Fig. 15c, L_1 and L_m fall on a narrow zone between two small circles the centre of which is determined from β-diagram for S_1 in the same domain (as shown in Fig. 15d). Therefore, in this small domain along the strike of S_1, it can be inferred that the lineation L_1 might have been originally constant in orientation and later displaced into the present orientation by superposed folding. In general, orientation of L_1 is more consistent along the horizon of rock sequence or the strike of S_1 than across them, and more variable or randum across them than along them. Domains which are homogeneous with respect to L_1 are generally very small.

b. Macroscopic analysis of L_2 and L_3

Fig. 16 shows a lineation diagram for L_2 in the domain I. Its pattern has a distinct maximum plunging 10° to N70°W. It coincides with the β-axis for S_1. In the domain II, lineation L_2 plunges steeply to S or SW, and is discordant with the β-axis for S_1. In the total domain, lineation L_2 is heterogeneous with respect to its orientation.

Pattern of lineation L_3 in the domain I shows a distinct maximum. Its plunge in the domain I is 10° to N71°W (Fig. 17a). Therefore, the maximum for L_3 coincides practically with that for L_2 but is discordant with the β-axis for S_1 in this domain. In the domain II (Fig. 17b), pattern of the lineation diagram for L_3 is similar to that in the domain I. The maximum for L_3 shows general plunge of 0° to N68°W. It coincides practically with the maximum for L_3 in the domain I. Therefore, maximum and pattern of the collective diagram (Fig. 17a) is concordant with those of the partial diagrams (Fig. 17a and b). The total domain can be regarded as homogeneous with respect to L_3.

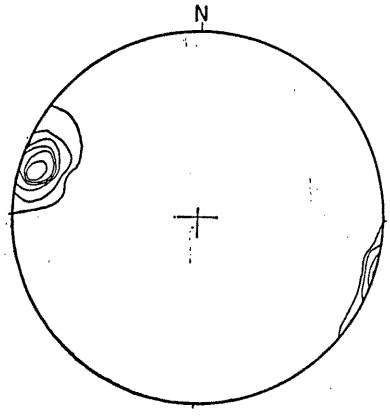

FIG. 16 Lineation diagram for L_2 in a small area at the Yakushitoge in the domain I. 60 points. Contours: 50-40-30-20-10-1%.

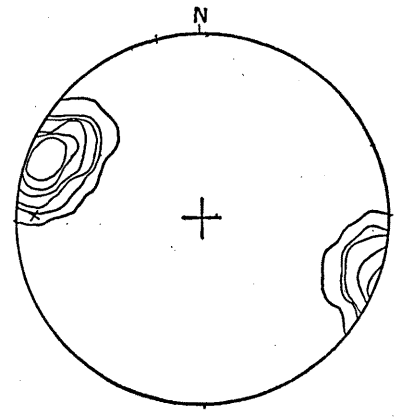

FIG. 17a Lineation diagram for L_3 of the domain I. A cross represents β_{S1} of the same domain detemined in Fig. 8. 863 points. Contours: 20-15-10-5-3-1%.

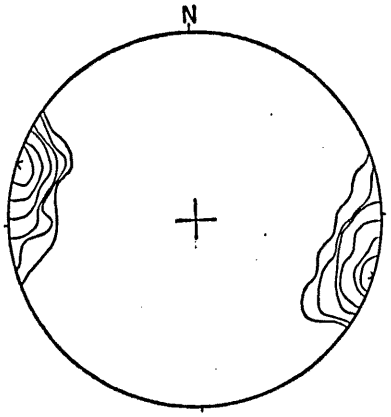

FIG. 17b Lineation diagram for L_3 of the domain II. A cross represents β_{S_1} of the same domain (Fig. 9). 150 ponts. Contours: 20-15-10-5-3-1%.

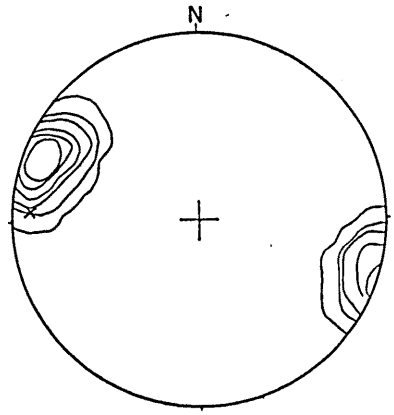

FIG. 17c Lineiation diagram for L_3 of the total domain. A cross represents β_{S_1} of the total domain (Fig. 6). 1005 points. Contours: 20-15-10-5-2-1%.

3. *Fold axes of type III and IV folds*

Orientation diagrams for axes of these types of folds are shown in Fig. 18a and b. A maximum in each diagram almost coincides with each other and is parallel to that of the lineation L_3. In this respect, axes of type III and IV folds are equivalent to L_3 in macroscopic geometry.

4. *Summary of macroscopic analysis in the large domain*

The present region is divided into two domains I and II with respect to β_{S_1}. The axis β_{S_1} in the domain I coincides with the axis of the Yakushi anticline and that in the domain II does with the axis of the Tsuneyama syncline. These two domains are not co-axial with respect to β_{S_1} but co-axial with respect to $\beta_{S_{2-2}}$, L_3, the β-axis for axial surfaces and the axis of type III and IV folds. The lineation L_1 and L_m

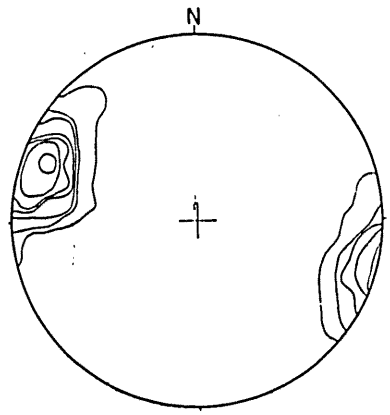

FIG. 18a Orientation diagram for axes of the type III and IV folds of the domain I. 115 points. Contours: 28-20-15-10-5-3-1%.

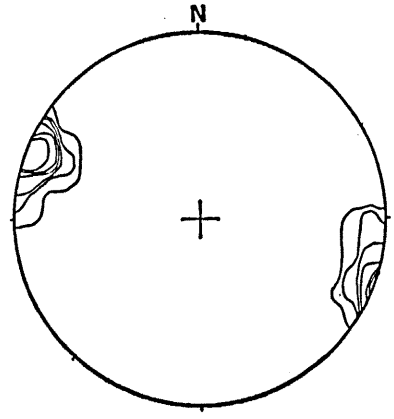

FIG. 18b Orientation diagram for axes of the type III and IV folds of the domain II. 52 points. Contnurs: 50-30-20-10-5-2%.

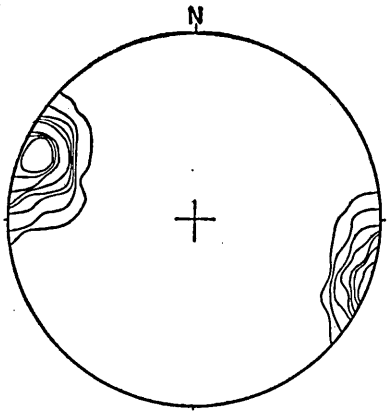

FIG. 18c Orientation diagram for axes of the type III and IV folds of the domain I and II. 167 points. Contours: 25-20-15-7-5-3-1%.

are variable in azimuth and plunge throughout the region, especially in the domain II. The orientation of L_2 is also discordant between the two domains.

B. MACROSCOPIC ANALYSIS IN THE HORIZON OF COUNTRY ROCKS OF THE SAZARE ORE DEPOSITS

As mentioned in the preceding pages of outline of geology and of mesoscopic analysis, lineations and folds with high angle plunge are developed in this domain. Galleries of the Sazare mine were cut on a certain horizon in which the bedded ore

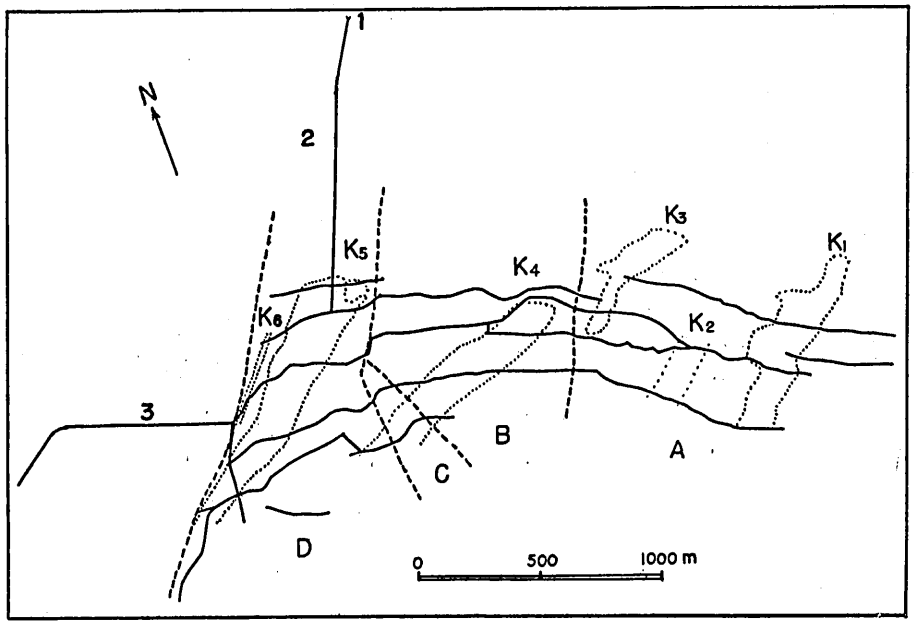

FIG. 19 Horizontal projection of main galleries, ore bodies, and domains (A, B, C, and D) for macroscopic analysis in the Sazare Mine. K_1 : Kinritsu ore body. K_2 : Kongo ore body. K_3 : Sazare ore body. K_4 : Kinsen ore body. K_5 : Kinsha ore body. K_6 : Shimpi ore body. 1 : Adit-entrance. 2 : Adit. 3 : Tomisatomuke prospecting gallery.

bodies exist. These galleries are favourable to observe fluctuation of linear structures on a certain horizon.

S-surfaces:—In Fig. 7a, *S*-pole diagram for S_1 in the small domain g, data of which are measured on the topographic surface, shows a somewhat divergent pattern in the direction E-W. This tendency is more distinct in the domain along the horizon of the Sazare ore deposits underground, as shown in Fig. 20a. As read from the pattern of the diagram, this domain seems to be fairly heterogeneous with respect to S_1-surfaces. Therefore, the domain must be subdivided into more homogeneous domains, i.e., A, B, C and D as shown in Fig. 19. In the domain A, the eastern part of the mine including the Kinsha-, the Kongo- and Kinritsu-ore bodies, strong

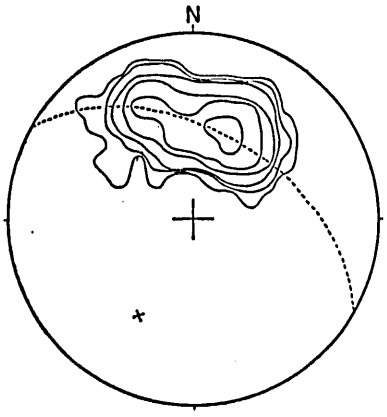

Fig. 20a S_1-pole diagram of basic and siliceous schists from the galleries of the Sazare Mine. Broken line shows π-circle for S_1. A cross represents β_{S_1}. 431 points. Contours: 10-7-5-3-2-1%.

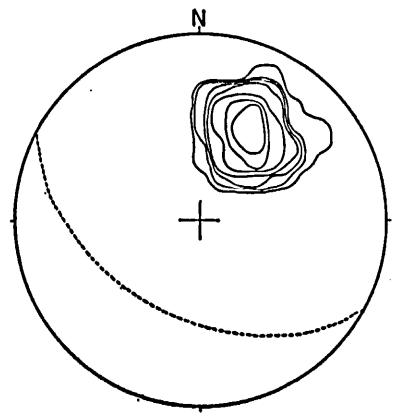

Fig. 20b S_1-pole diagram of the domain A. A broken line represents the general orientation of S_1 of the domain. 147 points. Contours: 20-15-10-5-3-2-1%.

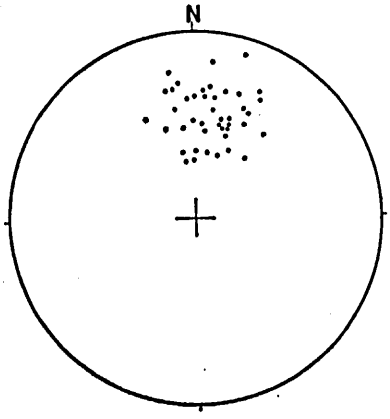

Fig. 20c S_1-pole diagram of the domain B. 44 points.

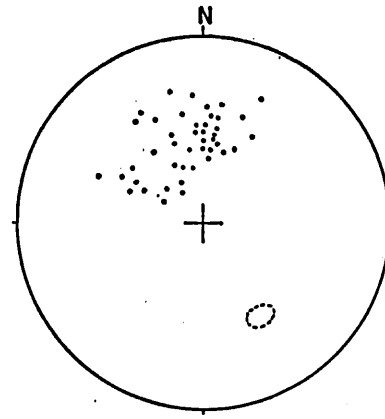

Fig. 20d S_1-pole diagram of the domain C. A broken line shows a maximum for β-diagram at the 18th level in the same domain. 44 points.

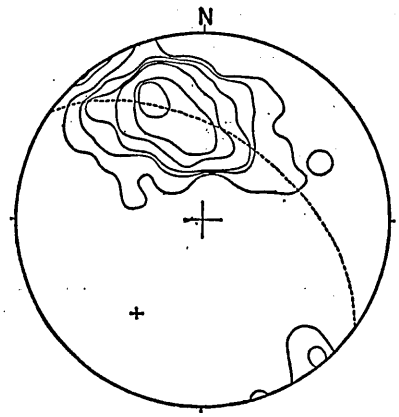

Fig. 20e S_1-pole diagram of the domain D. A droken line represents π-circle for S_1. A cross represents β_{s1}. 155 points. Contours: 15-10-5-3-2-1%.

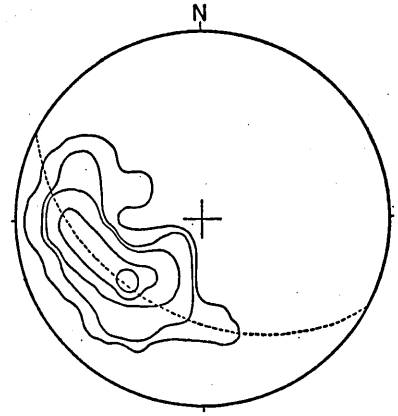

Fig. 21a Lineation diagram for L_1 of the domain A. A broken line represents the general orientation of S_1 in the domain. 110 points. Contours: 15-10-5-3-1%.

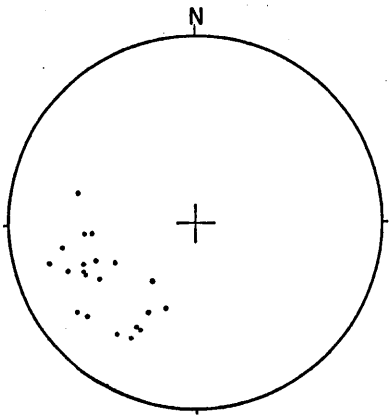

Fig. 21b Lineation diagram for L_1 of the domain B. 21 points.

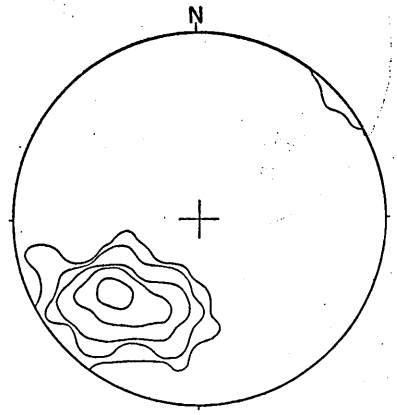

Fig. 21c Lineation diagram for L_1 of the domain D. 121 points. Contours: 20-10-5-3-1%.

concentration of poles of S_1-surfaces shows that S_1-surfaces are nearly plane (Fig. 20b). General strike is WNW (N60°W) and the dip is 46° to the south. The pattern elongated slightly in the direction N-S suggests that S_1-surfaces are slightly curved around the EW-axis. In the domain B, the central small part, S_1-surfaces strike almost E-W. In the domain C covering the part between the Kinsen-, and the Kinsha-ore bodies, β-axis for S_1 plunges 40° to S30°E as shown in Fig. 20d. It differs from the β-axis for S_1 in the domain of the Sazare mine (A, B, C and D). Finally in the domain D, which covers the Kinsha-, and the Shimpi-ore bodies, the β-axis for S_1 plunges to SW (38° to S35°W) (Fig. 20e). Therefore, β_{S_1} in the domain D is concordant with β_{S_1} determined from collective diagram in the domains A, B, C and D.

Lineations:—In the domain A, lineation L_1 is fairly variable in orientation as shown

in Fig. 21a. This pattern of lineation shows that L_1 swings on a plane surface of S_1. This tendency is also recognized in the domain B, as shown in Fig. 21b. In the domain D, however, concentration of L_1 and L_m is higher than in other domains (Fig. 21c). The type II folds with high angle plunge are observed in the domain D. The azimuth and plunge of L_2 are more or less parallel to L_1. Development of the type II folds and L_2 become stronger in the Tomisato fold.

C. Macroscopic Analysis of the Tomisato Fold

In the west of Kinsha ore body, a complex fold named the Tomisato fold has been discovered by Doi (1959) and by Hirata (1959).

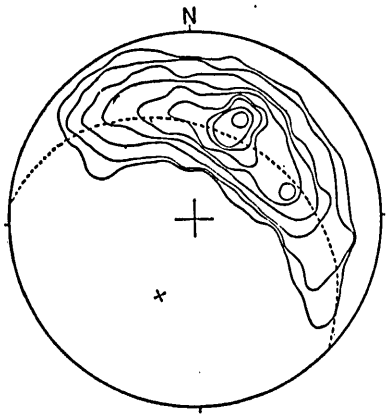

Fig. 22 S_1-pole diagram of the Tomisatomuke prospecting gallery. A broken line shows a small circle with angular radius 77° and the cross shows the centre of the small circle. 1089 points. Contours: 9-7-6-5-4-3-2-1%.

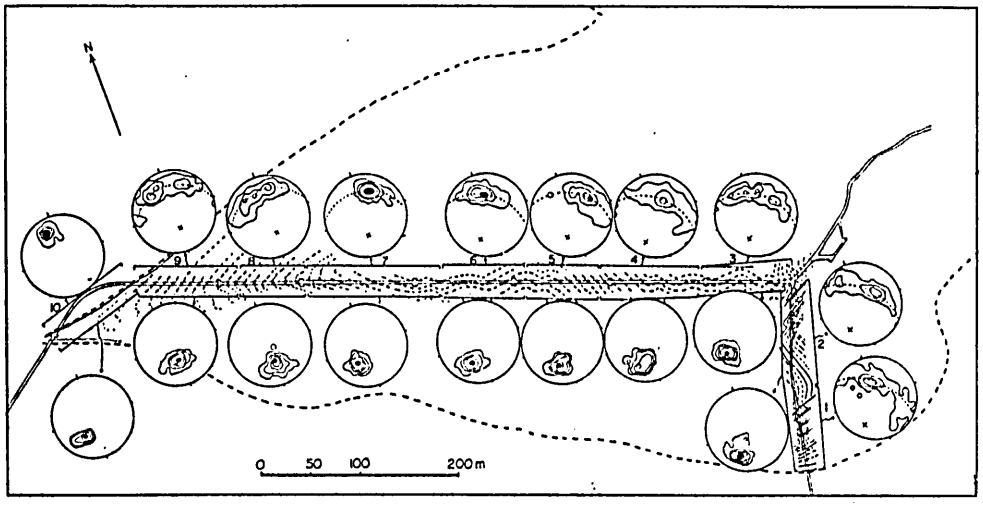

Fig. 23 Structural sketch map and orientation data for S_1 and lineations in subareas in the Tomisatomuke prospecting gallery.

Diagrams on the upper side are those for S_1-pole. The cross in each S_1-pole diagram shows β_{S_1} in each subarea. Lineation diagrams are shown on the lower side. Contours: 30-20-10-5-1%.

Poles of S_1-surface measured at the Tomisatomuke prospecting gallery fall on a small circle girdle in the collective diagram as shown in Fig. 22. This pattern of S_1-pole diagram indicates that the domain covering the Tomisato fold is heterogeneous with respect to β_{S_1}. It suggests two cases with respect to geometry of the Tomisato fold, that is, whether the fold form of the Tomisato fold is conical or the fold axis of the Tomisato fold is very variable in orientation. To test this problem the domain of the Tomisato fold is divided into ten smaller areas, as shown in Fig. 23. In each area, the S_1-pole diagram shows a relatively well developed great circle girdle. This suggests strong development of small scale folds in the Tomisato fold. In the synoptic diagram of β_{S_1} (Fig. 24), β_{S_1} in these subareas falls into two groups, and the plunge of β_{S_1} of the subareas 1 to 7 varies gradually from 30° toward S40°W to 50° toward S12°W, but sudden change in orientation of β_{S_1} can be recognized between the subareas 7 and 8. The gradual and sudden change of orientation of β_{S_1} suggests that the fold form of the Tomisato fold is convergent downwards as a cone shape. The form of the fold, however, may not be the ideal cone shape as shown in the underground geological map.

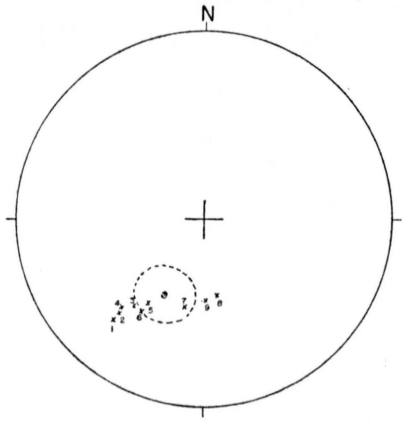

Fig. 24 Synoptic diagram for β_{S1}. The cross represents β_{s1} of each S_1-pole diagram in Fig. 23. A broken line shows small circle of the angular radius of 13° the centre (circled cross) of which is determined in Fig. 22.

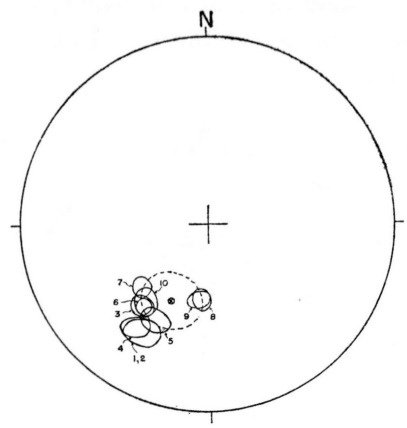

Fig. 25 Synoptic diagram for lineations. Full lines with numbers 1~10 show respective maximum areas (30%) of each lineation diagram in Fig. 23. A broken line shows a small circle with angular radius of 13° (circled cross) of which is determined in Fig. 22.

Diagrams for lineations L_1, L_m and L_2 in each subarea are shown in Fig. 23. Most lineations fall on the southwest quadrangle in each diagram. The maximum in each diagram falls into two groups as shown in the synoptic diagram (Fig. 25). In the subareas 1 to 7 which are the east part of the Tomisato fold, lineations plunge generally SW to SSW, while in the subareas 8 and 9 lineations plunge to due south. Two groups of maxima in those subareas are concordant with those of β_{S_1}. It must be noticed that the maximum of lineation diagram in each subarea lies on a small circle girdle with angular radius of 13°.

The axes of small-scale type II folds (B_2) in the gallery fall on a wide area in Fig. 26b, which covers the areas for lineations and β_{S_1}. Axial surfaces in the areas 8 and 9 are parallel to the axial surface of the Tomisato fold in the west part.

From macroscopic analysis of S_1 and lineations, the form of the Tomisato fold can be considered to be a distorted cone-like form. Two groups for β_{S_1} or lineations in synoptic diagrams suggests that the Tomisato fold is composed of two domains, that is the eastern domain which covers the subareas 1 to 7 and the western domains which covers the subareas 8 and 9. The eastern domain represents the east hinge and the western domain the west hinge. In the eastern domain, β_{S_1} and lineations plunge moderately southwestward, while in the western domain those plunge steeply southward. Therefore, the Tomisato fold has two fold axes which are mutually oblique and convergning downwards. As mentioned in the mesoscopic analysis, the small-scale folds which are predominating in the hinge zones of the Tomisato fold belong to the type II folds. The Tomisato fold shows style of the type II folds. Therefore, the present fold form of the Tomisato fold might have been formed in the stage of the formation of the type II folds. It can be inferred, however, that the folding movement in this domain might have been started at early stage (the stage of the formation of the type I folds), because B_1, L_1, and L_m are also parallel to B_2 and L_2.

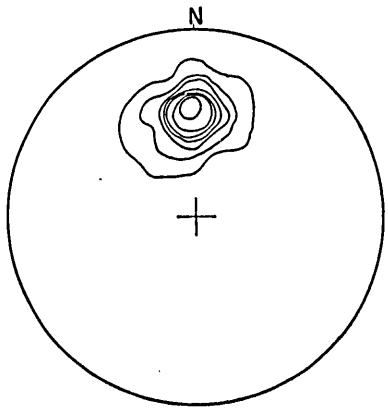

Fig. 26a *s*-pole diagram for axial surfaces of small scale folds of the Tomisatomuke prospecting gallyery. Contours: 26-22-18-14-10-6-2-%.

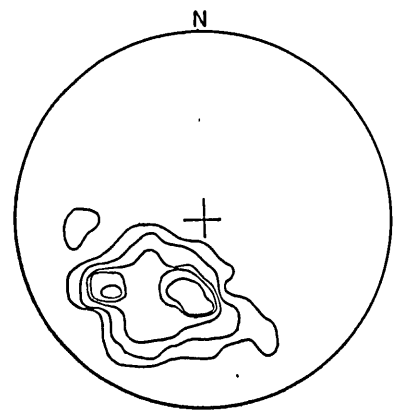

Fig. 26b Axes of smallscale folds of the Tomisatomuke prospecting gallery.

In the domain D which covers the Kinsha ore body, small-scale folds with SW-plunge are well developed and ore shoot is greatly controled by these folds. The β_{S_1} in the domain D coincides with that in the eastern part of the Tomisato fold. Therefore, macroscopic structures in the domain D are concordant with the Tomisato fold. Furthermore, S_1-surfaces in the larger domain including domains A, B, C and D are practically tautozonal with those in the domain D in the eastern part of the Tomisato fold. From these geometric relations, the formation of the Tomisato fold

may be closely related to that of the fold structures in the domain D as well as that of the moderately curved structures of the ore horizon of the Sazare mine.

VI. Microscopic Analysis

A. Microscopic Descriptions

1. *Relation between metamorphic minerals and micro-scale structures.*

In pelitic, psammitic, and siliceous schists, micro-scale lamination composed of micarich layers and quartz-rich layers is developed. Basal cleavage planes {001} of micas and chlorites are oriented a most parallel to S_1 in mica-rich layer. It can be observed, however, that isoclinal folds (type I folds) of S_1-surfaces are sometimes developed on a micro-scale. In this case, basal cleavages of micas and chlorites are oriented parallel to the axial surface of the type I folds. These attitudes of phyllosilicates around the type I folds are shown in Fig. 27a. Orientation patterns will be presented in the next section (page 322).

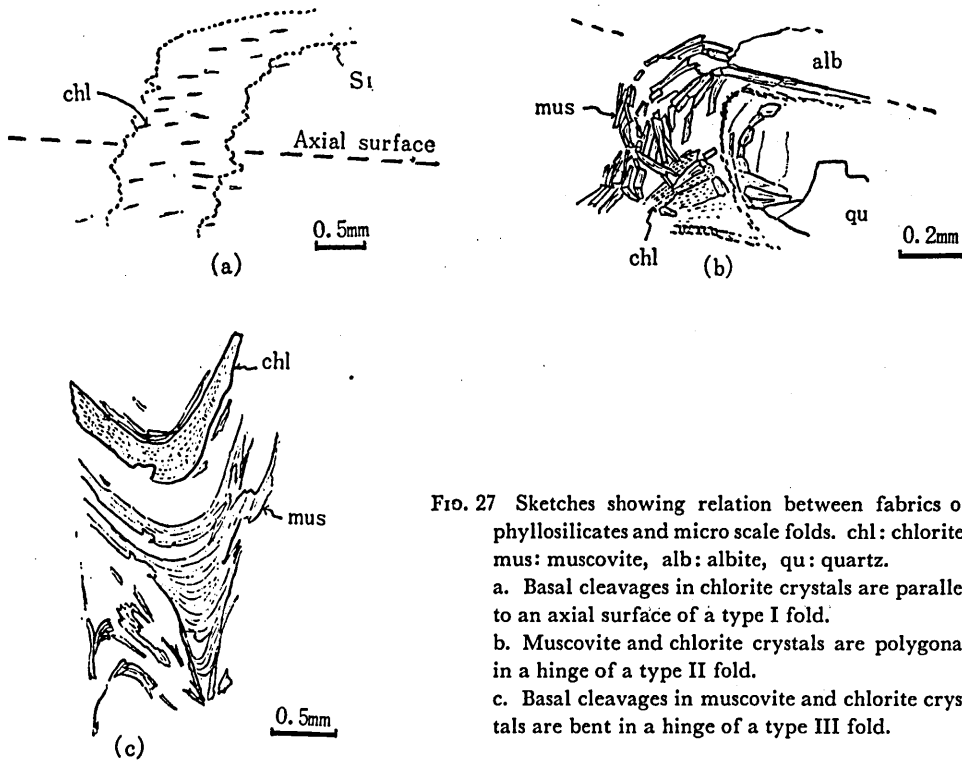

Fig. 27 Sketches showing relation between fabrics of phyllosilicates and micro scale folds. chl: chlorite, mus: muscovite, alb: albite, qu: quartz.
a. Basal cleavages in chlorite crystals are parallel to an axial surface of a type I fold.
b. Muscovite and chlorite crystals are polygonal in a hinge of a type II fold.
c. Basal cleavages in muscovite and chlorite crystals are bent in a hinge of a type III fold.

In the type II folds, micas and chlorites are rarely bent but show polygonal texture around the hinge of the micro-scale folds. Orientation of {001} in mica is fairly controled by the form surface of the type II folds (Fig. 27b).

Basal cleavages of micas and chlorites adjacent to the cleavage surface S_{2-2} are

bent or twisted adjacent to S_{2-2} or at the hinge of micro-scale folds of type III and IV, as shown in Fig. 27c. The S_{2-2}-surfaces are generally related to the type III and IV folds. In most cases, it occurs as a single set but sometimes as conjugate sets of transversal cleavages. It occurs generally in mica- and chlorite-rich layers and is often obscured in quartz rich layers. When slip is recognized on S_{2-2}, relative slip sense on S_{2-2} can be defined in the domain of thin section but is not constant in larger domains.

2. *Porphyroblasts*

Development of porphyroblasts of metamorphic minerals such as albite, amphibole, chlorite, stilpnomelane, tourmaline, etc. can be observed in the metamorphic zones II and III. Albite is the most conspicuous among them.

Grain dimension of albite porphyroblasts ranges from 0.2 mm to 1 cm with rounded or ellipsoidal shape. The shortest axis is in general nearly parallel to the fabric axis c. Inclusions in porphyroblasts have been discussed widely (READ, 1949; TURNER and VERHOOGEN, 1951; ZWART, 1960). Trends of dark inclusions in albite porphyroblasts show conspicuous fold forms. Some of them are isoclinal folds (Fig. 3 in Plate 30) and micro-scale folds with cleavages (Fig. 4 in Plate 30). These patterns can neither be regarded as spiral trends formed synchronously with crystallinzation of albite nor as formed after crystallization. Therefore, folded trend of inclusions can be considered to have existed before crystallization of albite. These structures can be identified with the type I folds. In most cases, trends (s_i in Sander's sense) of dark inclusions in albite porphyroblasts are not continuous to external S-surfaces (s_e).

The observation described above suggests that some albite porphyroblasts have been crystallized after the type I folds. In stilpnomelane porphyroblasts, helicitic structures inherited from external S_1-surface are observed in pelitic schists near the contact with ultra-basic rocks at the Dozan River. In amphibole and tourmaline, inclusions of epidote, quartz, hematite, rutile are observed.

B. PREFERRED ORIENTATION OF METAMORPHIC MINERALS

Preferred lattice and dimensional orientation of metamorphic minerals such as amphiboles, epidotes, micas, chlorites, quartz, tourmaline, and hematite are conspicuous in the Sambagawa crystalline schists. In this district, tourmaline tabrics were already reported (OYAGI, 1963). The data of main constituent minerals will be described.

In petrofabric descriptions, fabric axes will be set up as follows: the fabric axis b is parallel to L_1 or B_1, the fabric axis a is normal to b on S_1 and the fabric axis c is normal to a and b.

1. *Amphiboles*

Amphiboles in the metamorphic zone I are glaucophanic amphibole and actinolitic amphibole. They are small in grain size (0.01～0.1mm). Therefore, lattice orientation is not determined directly. Actinolitic amphibole is accicular in shape elongated

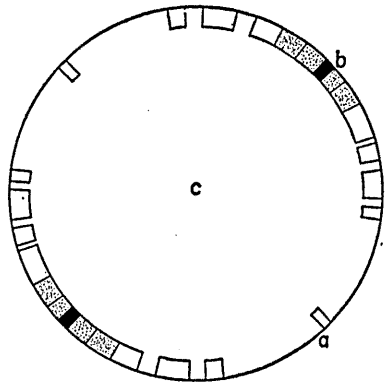

FIG. 28 Azimuth for *c*-axes in actinolite of basic schist from southwest of Yakushitoge, 100 grans. Contours: 15-10-5-1%.

parallel to the crystallographic *c*-axis. Therefore, lattice orientation and dimensional orientation coincide mutually. Concentration of *c*-axes of actinolitic amphibole is parallel to L_1, and L_2 as shown in Fig. 28. Glaucophanic amphibole, however, is irregular in shape and in orientation than actinolitic amphibole. In the zone IIa, pattern of lattice and dimensional orientation of amphibole is not different from that in the zone I and *c*-axes of amphibole are parallel to L_1 which trends WNW with shallow plunge. In the zone IIb, amphiboles (glaucophanic amphiboles, barroisitic hornblende, etc.) show distinct preferred orientation in lattice and dimension. Four examples will be described.

Specimen 1. (N059XI14-1)

Piedmontite-colourless glaucophane-muscovite-quartz-schist, collected from 400m west of the Kinsha ore body on the 6th sublevel. The locality is situated stratigraphically in the Upper member of the Minawa formation, structurally on the south limb of the Yakushi anticline and in the eastern part of the Sazare mine (the domain D of macroscopic analysis). S_1-surface is distinct by compositional banding. Lineation L_1 is also distinct and plunges 70° to S40°W; lineation normal to L_1 is very weak. Optic ellasticity axes X, Y, and Z of amphoboles are measured and the results are shown in Fig. 29.

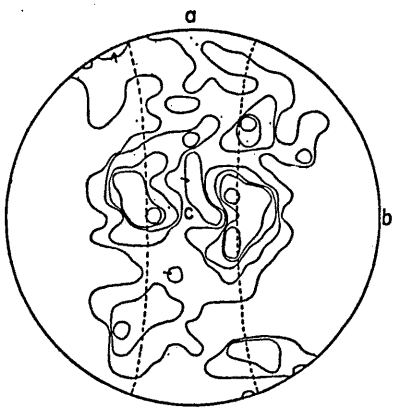

FIG. 29a Orientation diagram for X-axes in colourless glaucophane in specimen 1 (siliceous schist). 200 grains. Contours: 5-4-3-2-1%.

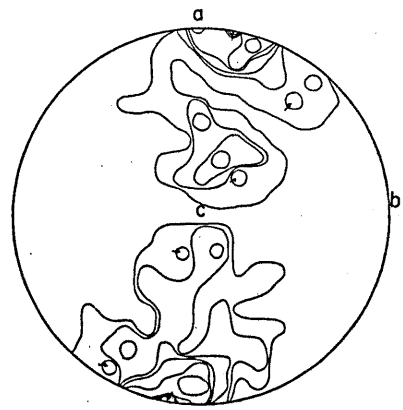

FIG. 29b Orientaion diagram for Y-axes in colourless glaucophane in specimen 1. 200 grains. Contours: 6-5-4-3-2-1%.

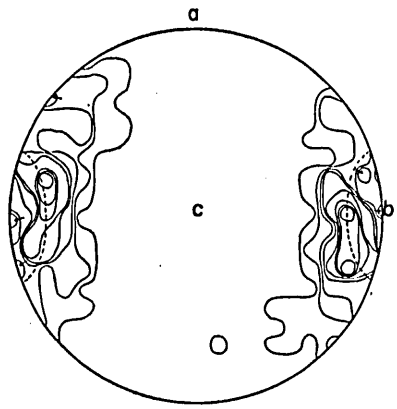

Fig. 29c Orientation diagram for Z-axes in colourless glaucophane in specimen 1. 200 grains. Contours: 8-7-6-5-4-3-2-1%.

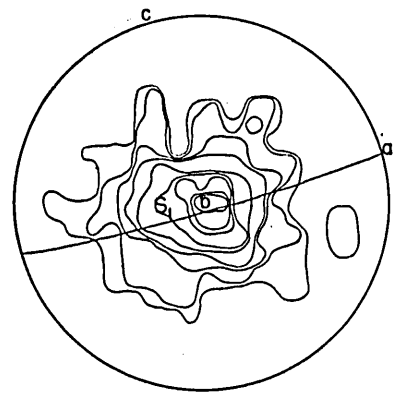

Fig. 30a Orientation diagram for [001] in glaucophanic amphibole in specimen 2 (siliceous schist). 200 grains. Contours: 16-12-9-7-5-3-2-1%.

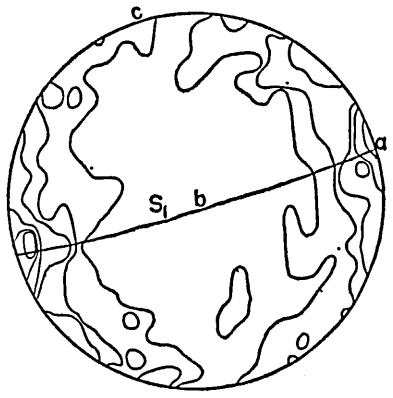

Fig. 30b Orientation diagram for Y-axes in glaucophanic amphibole in specimen 2. 150 grains. Contours: 5-4-3-2-2/3%.

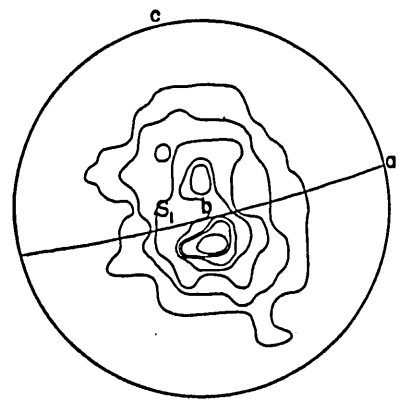

Fig. 30c Orientation diagram for Z-axes in glaucophanic amphibole in specimen 2. 150 grains. Contours: 12-10-8-6-4-2-2/3%.

Specimen 2. (N058V27-7)

Glaucophanic amphibole-muscovite-quartz-schist, collected from 400m south of the horizon of the Sazare mine at the west side of the Kamiogawa Valley. The locality is situated stratigraphically in the Upper member of the Minawa formation, somewhat upper than specimen 1. S_1-surface is well developed with parallel arrangement of white mica and compositional banding. Small-scale isoclinal folds are observed at the locality and in the specimen. L_1 is parallel to isoclinal fold axis and is distinct. Optic ellasticity axes X, Y, and [001]-axes of amphibole are measured and the results are shown in Fig. 30.

Specimen 3. (N058IX12-4)

Bluish green amphibole-epidote-muscovite-quartz-schist, collected from the Tomisatomuke prospecting gallery on the 12th level of the Sazare mine. The locality is situated in the Upper member of the Minawa formation, almost the same horizon as the specimen 1, structurally on the south limb of the Yakushi anticline, and on the eastern hinge of the Tomisato fold. S_1 is distinct. Lineation L_1 is clear on S_1 and plunges 24° to S40°W. Long axis of amphibole is parallel to L_1. Lineation oblique

to L_1 is very weak. A set of transversal schistosity-surfaces is well recognized by mica orientation. Optic ellasticity axes X, Y, and Z are measured and the results are shown in Fig. 31.

Specimen 4. (N058VI13-6)

Spotted basic schist (bluish green amphibole-epidote-chlorite-albite-schist), collected from the Tomisatomuke prospecting gallery on the 12th level. The locality is situated in the Upper member of the Minawa formation, lower than specimen 3; structurally on the south limb of the Yakushi anticline and on the west hinge of the Tomisato fold. S_1 is relatively distinct. Micro-scale isoclinal fold are observed on the section and small-scale folds are intensively developed at the locality. Lineation L_1 is well developed and lineations oblique to L_1 are observed (Fig. 32).

In specimen 1 (Fig. 29), Z-axes of colourless glaucophane fall on a small circle girdle with angular radius 18°, and X-axes on a small circle girdle with angular radius 72°. Y-axes fall on a great circle girdle. These small and great circles are coaxial. The centre of these circles coincides with the lineation L_1. The pattern of orientation that the maxima of Z-axes fall near *bc*-plane and the maxima of Y-axes

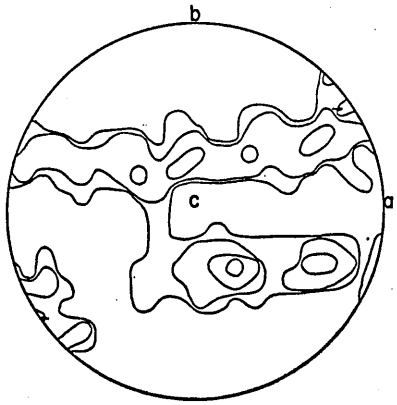

Fig. 31a Orientation diagram for X-axes in bluish green amphibole in specimen 3 (spotted basic schist). 150 grains. Contours: 6-4-2-4/3%.

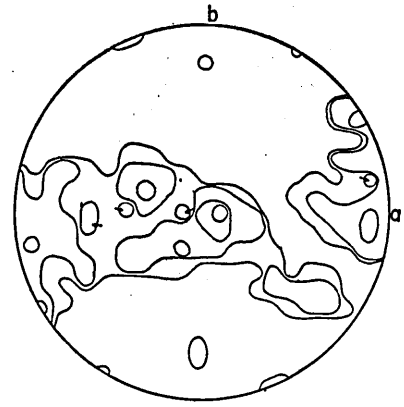

Fig. 31b Orientation diagram for Y-axes in bluish green amphibole in specimen 3. 150 grains. Contours: 6-4-2-4/3%.

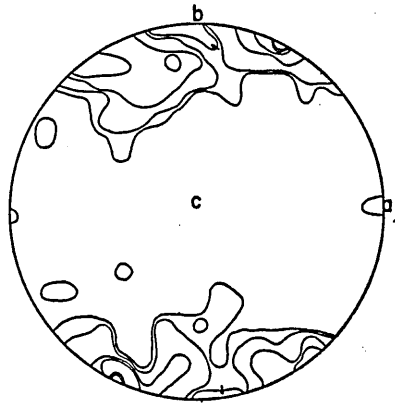

Fig. 31c Orientation diagram for Z-axes in bluish green amphibole in specimen 3. 150 grains. Contours: 10-8-6-4-2-4/3%.

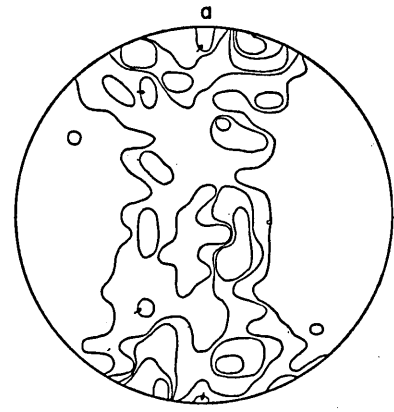

Fig. 32a Orientation diagram for X-axes in bluish green amphibole in specimen 4 (spotted basic schist). 200 grains. Contours: 5-4-3-2-1%.

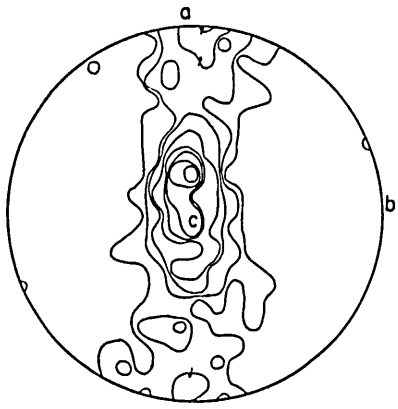

Fig. 32b Orientation diagram for Y-axes in bluish green amphibole in specimen 4. 200 grains. Contours: 8-7-6-5-4-3-2-1%.

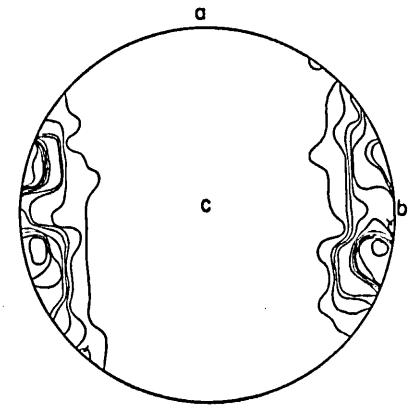

Fig. 32c Orientation diagram for Z-axes in bluish green amphibole in specimen 4. 200 grains. Contours: 12-10-8-7-6-5-4-3-2-1%.

near the fabric axis *a* is consistent with the rule proposed by Sander (1930), Ishioka and Suwa (1954) and Kojima and Hide (1957). In specimen 2 (Fig. 30), the maximum of [001]-axes of amphibole coincides with the lineation L_1 (fabric axis *b*), and Y-axes fall on surface S_1. This pattern is the same as that of specimen 1. In specimen 3 (Fig. 31), orientation pattern suggests that [001] of amphibole is parallel to L_1. Reason for weak concentration of Y-axes and X-axes is not clear. In specimen 4 (Fig. 32), [001]-axes of bluish-green amphibole are suggested to be parallel to L_1. The orientation pattern of Y-axes, however, suggests that {100} are oblique to the surface S_1. In this specimen, as the surface S_1 is the enveloping surface of well developed micro-scale folding, the S_1-surface in micro-scale domain is oblique to the enveloping surface. Therefore, orientation rule of amphibole in this specimen is also consistent with that of the other specimens. From these discussions, it is clear that the orientation of amphiboles is chiefly controled by L_1 or B_1 (the axis of the type I fold) and the surface S_1.

2. *Epidotes*

As for the orientation rule of epidote, preferred orientation of [010]-axis (=Y-axis) parallel to the fabric *b*-axis has been agreed by many authors (Sander, 1930; Ladurner, 1954; Kojima and Hide, 1958; Turner and Weiss, 1963). Two cases, however, have been demonstrated with respect to preferred orientation of crystallographic planes on S-surface. Orientation of {001} parallel to *ab*-plane has been demonstrated by Ladurner and Turner and Weiss, while that of $\{10\bar{2}\}$ parallel to S_1 is reported by Kojima and Hide (1958). In the zones I, and IIa, measurements of optic elasticity axes or of crystallographic planes are impossible, because grain size of epidotes is very small and show rounded shape as described in page 9. However, it can be observed on thin sections that the longest dimension of epidotes is generally parallel to L_1 or B_1 when the grain size of epidote is inequidimensional. Some examples for orientation data will be described from the zone IIb.

Specimen 5. (N061IX15-1)

Piedmontite-colourless glaucophane-muscovite-albite-quartz schist, collected from the same locality as specimen 1. Geological situation and rock structures are the same as specimen 1.

Optic elasticity axes X, Y, and Z in 100 piedmontite grains are measured. In Fig. 33b, Y-axes concentrate near the lineation L_1 ($=b$), while X-axes and Z-axes fall on great circle girdle (Fig. 33a and c), respectively. In this specimen, orientation of Y-axes (crystallographic b-axis) is concordant with the orientation rule reported by many authorts.

Specimen 6. (N059I29-2)

Epidote-muscovite-albite-quartz schist, collected from 90m east of the Kinsha ore body on the 6th sublevel. The locality is on the same horizon as the specimen 1, in the central part (domain B) of the Sazare mine. Schistosity surface S_1 is well developed. Lineation L_1 and other lineations are weak. Small and micro-scale-folds are not recognized in the specimen.

The maximum of Y-axes is almost parallel to the lineation L_1 ($=b$) (Fig. 34b). In Fig. 34a and c, X-axes and Z-axes fall on a great circle girdle with widely distributed maxima and submaxima. Therefore, preferred orientation of unique planes is lacking.

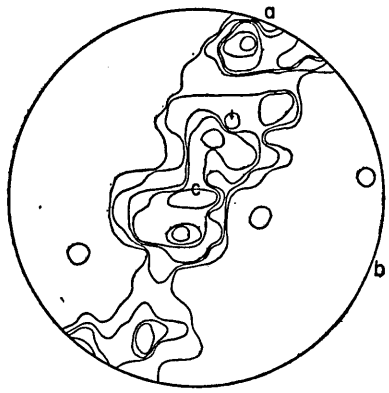

Fig. 33a Orientation diagram for X-axes in piedmontite in specimen 5 (spotted siliceous schist). 100 grains. Contours: 8-6-4-3-2-1%.

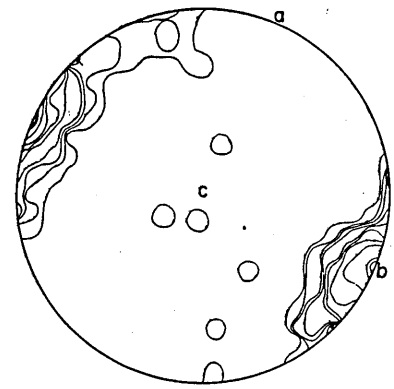

Fig. 33b Orientation diagram for Y-axes in piedmontite in specimen 5. 100 grains. Contours: 22-18-14-10-6-4-2-1%.

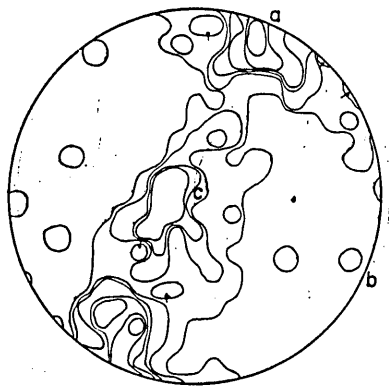

Fig. 33c Orientation diagram for Z-axes in piedmontite in specimen 5. 100 grains. Contours: 8-6-4-3-2-1%.

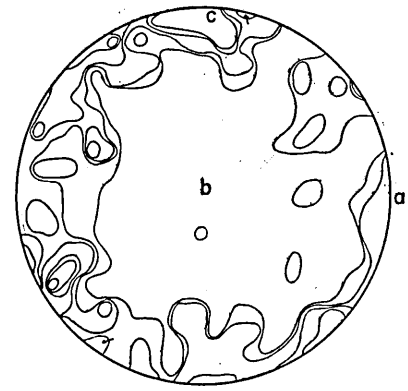

Fig. 34a Orientation diagram for X-axes in epidote in specimen 6 (spotted siliceous schist). 100 grains. Contours: 6-5-4-3-2-1%.

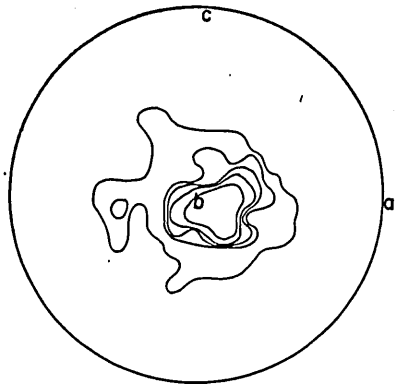

Fig. 34b Orientation diagram for Y-axes in epidote in specimen 6. 100 grains. Contours: 10-8-6-4-2%.

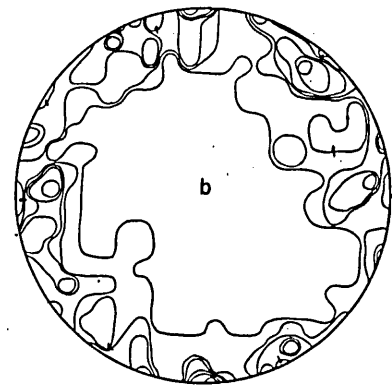

Fig. 34c Orientation diagram for Z-axes in epidote in specimen 6. 100 grains. Contours: 6-5-4-3-2-1%.

Specimen 7. (N058IX15-8)

Piedmontite-muscovite-quartz-schist, a country rock of the Kinsha ore body on the 12th level in the Sazare mine. The locality is almost the same horizon as the specimen 6. S_1 is less developed than in other specimens. Lineation L_1 is distinct but other lineations are weak. Most epidote grains show zonal structure in which the core of the grain is piedmontite and the periphery is pistacite as reported by Iwasaki (1960). Birefringence is larger in the core than in the periphery of the grain. Grain shape of epidote is elongated parallel to the crystallographic *b*-axis.

In Fig. 35b, Y-axes concentrate chiefly near L_1, but some deviation is recognized. X-axes and Z-axes fall on a great circle girdle but unique concentration is lacking on them (Fig. 35a and c). Weak preferred orientation will be due to micro-scale folds developed in this specimen.

Specimen 8. (N061VIII31-1)

Piedmontite-quartz schist, collected from a locality 1700m north of Fujiwara (1km west of the Sazare mine). The locality is situated stratigraphically in the Upper member of the Minawa formation and structurally on the steeply dipping south limb of the Yakushi anticline. S_1 is distinct. The type I folds on a small scale are recognized and axial surfaces of the folds are parallel to S_1. Lineation L_1 and axes of the type I folds are clear and mutually parallel. Lineations across L_1 are not observed in

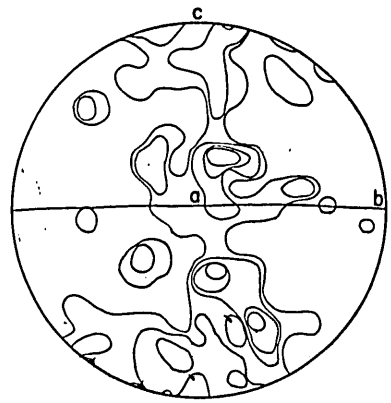

Fig. 35a Orientation diagram for X-axes in epidote in specimen 7 (spotted siliceous schist). 150 grains. Contours: 4-3-2-1%.

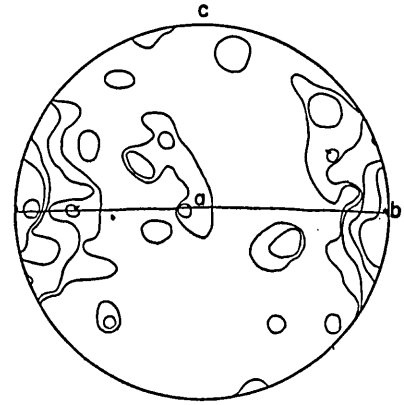

Fig. 35b Orientation diagram for Y-axes in epidote in specimen 7. 150 grains. Contours: 8-6-4-2-1%.

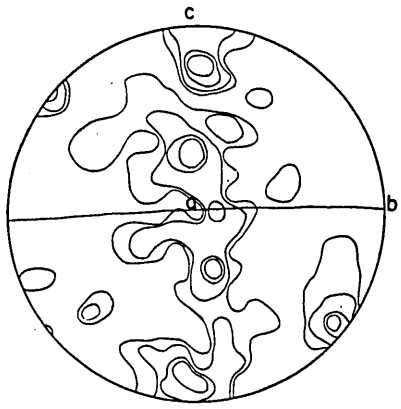

FIG. 35c Orientation diagram for Z-axes in epidote in specimen 7. 150 grains. Contours: 4-3-2-1%.

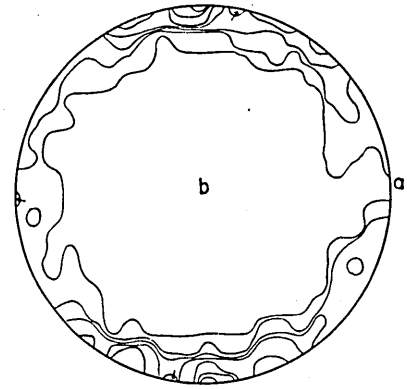

FIG. 36a Orientation diagram for X-axes in piedmontite in specimen 8 (folded spotted siliceous schist). 200 grains. Contours: 10-8-6-4-3-2-1%.

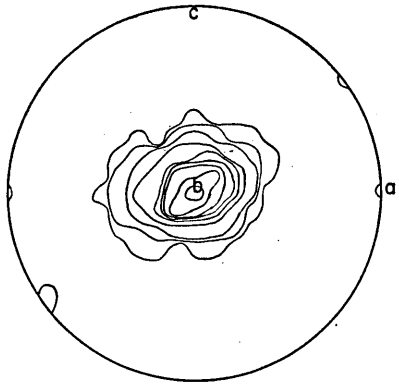

FIG. 36b Orientation diagram for Y-axes in piedmontite in specimen 8. 200 grains. Contours: 20-15-12-10-8-6-4-2-1%.

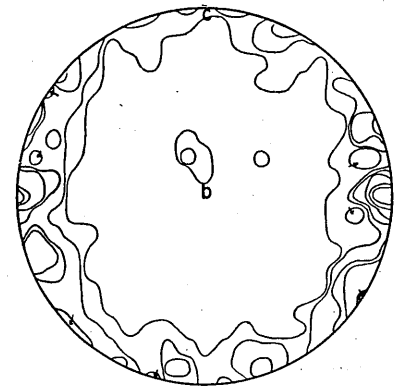

FIG. 36c Orientation diagram for Z-axes in piedmontite in specimen 8. 200 grains. Contours: 8-6-4-3-2-1%.

this specimen but developed in the area of the locality. Main component minerals are piedmontite, muscovite, chlorite and quartz. Piedmontite shows pleochloism with X=yellow, Y=pink and Z=red. Grain shape of some piedmontite grains show wedge- or parallelogram-form with well developed $\{10\bar{2}\}$ in *b*-section like the mineral reported by KOJIMA and HIDA (1958).

In Fig. 36b, Y-axes coincide clearly with L_1 and the axis of the type I fold. Orientation for X- and Z-axes is characterized by *ac*-girdle as in other specimens, but a maximum is recognized (Fig. 36a and c). The maximum for Z-axes coincides the fabric axis *a* and that for X-axes coincides the fabric axis *c*. This pattern shows that $\{10\bar{2}\}$-planes are nearly parallel to the axial surface of the fold as described by KOJIMA and HIDE (1958).

In the zones I and IIa, long dimension of epidotes is parallel to L_1 (and L_2). In four examples of the zone IIb, the crystallographic *b*-axis (=optic elasticity axis Y) is oriented parallel to L_1 (=*b*-fabric axis). In specimens 8, $\{10\bar{2}\}$-planes are oriented parallel to the axial surfaces of the type I folds. From these data, it may be clear that orientation of epidotes is chiefly controled by the lineation L_1 and the axial

surface of the type I fold in the crystalline schists of this region.

3. *Mica.*

Optic elasticity axes of muscovite are measured only for a single specimen, and its preferred orientation is consistent with that so far reported. In many specimens, orientation diagrams for {001}-poles of muscovite and chlorites were prepared. These data are shown along with quarts fabrics of respective specimens.

Specimen 5. (N061IX15-1)

This specimen is the same one for which orientation of epidote was measured. Muscovite is more or less flexured around hinge zones of the micro-scale type III folds and the dimension of mica grains is from 0.1mm to 1mm. Optic elasticity axes, X-, Y-, and Z-axes, in 200 muscovite grains were measured on *c*-section. In Fig. 37a, X-axes fall on a partial girdle which coincides with the girdles for X- and Z-axes of piedmontite (cf. Fig. 33a and c).

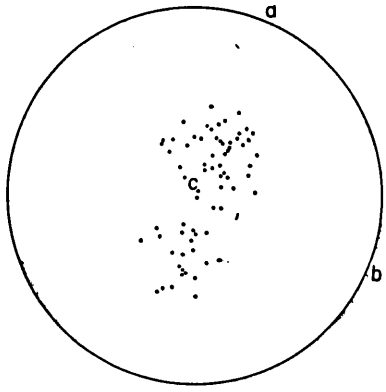

Fig. 37a Orientation diagram for X-axes in muscovite in specimen 5 (spotted siliceous schist). 70 grains.

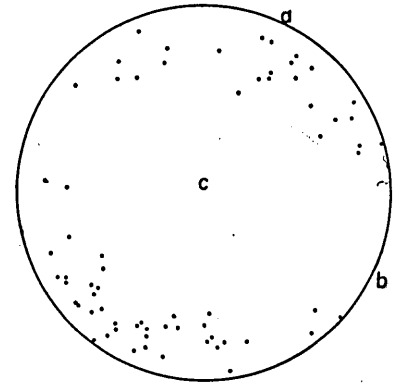

Fig. 37b Orientation diagram for Y-axes in muscovite in specimen 5. 70 grains.

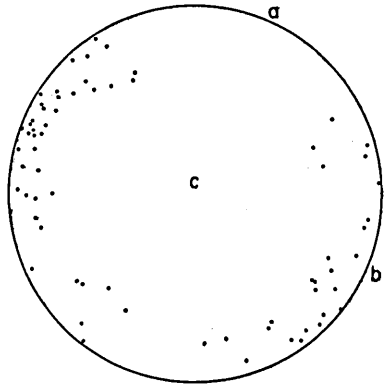

Fig. 37c Orientation diagram for Z-axes in muscovite in specimen 5. 70 grains.

Although concentration is weak, Y-axes tend to concentrate to the fabric axis *a* and Z-axes concentrate to the fabric axis $b(=L_1)$ (Fig. 37b and c).

It is shown that {001}-poles for mica and chlorites are normal to the schistosity-

surface S_1 in most orientation diagrams. It suggests that basal cleavages for these minerals are parallel to the surface S_1. In general, {001}-poles fall on a partial girdle the pole of which coincides with L_1 (fabric axis b). On thin sections normal to L_2 are observed weakly developed conjugate sets of transversal schistosity-surfaces the intersection of which is parallel to L_2 on S_1. These surfaces are suggested in diagrams by elongated contour lines (2%–6%) on *ac*-plane (Fig. 45a) or submaxima of concentration (Fig. 44a).

4. *Quartz*

In this section, orientation pattern of quartz [0001]-axes will be treated from various horizons, metamorphic zones and structural positions, from the Yakushi anticline to the Tsuneyama syncline.

Specimen 9. (N059I25-5)

Psammitic schist, collected from the locality west of Yakushitoge. The locality is situated stratigraphically in the lower member of the Minawa formation and structurally on the north limb of the Yakushi anticline near the crest. It belongs to be the zone I of mineral zoning. The surface S_1 is distinct and the transversal schistosity-surface S_{2-2} is weak. The lineation L_3 is recognized on S_1. Main component minerals are muscovite, quartz and albite. Quartz is small in grain size except those derived probably as clastic minerals. Muscovite is rich in this specimen.

Orientation diagram for quartz shows weak preferred orientation (Fig. 38). Four maxima of weak concentration are situated symmetrically near the periphery (=*ac*-plane). The symmetry of the diagram is nearly orthorhombic with respect to maxima.

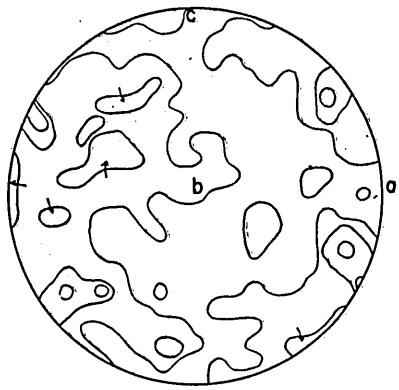

Fig. 38 Orientation diagram for [0001] in quartz in specimen 9 (psammitic schist), 400 grains. Contours: 3-2-1%.

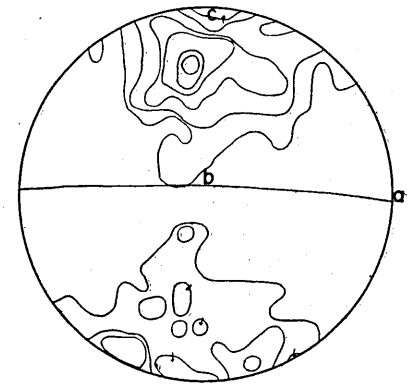

Fig. 39 Orientation diagram for [0001] in quartz in specimen 10 (siliceous schist), 400 grains Contours: 6-5-4-3-2-1%.

Specimen 10. (N058V28-6)

Siliceous schist, east of the Sazare mine. The locality is situated in the middle member of the Minawa formation and structurally on the south limb of the Yakushi anticline. The surface S_1 is distinct and S_{2-2} is weak. The lineation L_1 and L_3 is recognized on S_1. Component minerals are quartz, albite, muscovite and chlorite.

In this specimen, quartz [0001]-axes show strong preferred orientation (Fig. 39). One distinct maximum and two submaxima fall on the position 20°~30° from the

fabric axis *c*, apart from *ac*-plane. In this diagram, the quartz diagram has a triclinic symmetry, having stronger concentration on the upper left part.

Specimen 11. (N059I20-1)

Pelitic schist, 59m south of the adit-entrance of the Sazare mine. The locality is situated stratigraphically on the lower horizon of the upper member of the Minawa formation, and structurally on the south limb of the Yakushi anticline. It belongs to the zone I of mineral zoning. The surface S_1 is distinct and cleavage S_{2-2} is clearly observed on thin section. The lineation L_1 and L_3 are slightly oblique (10°~20°). The former is faint and the latter is clear.

An incomplete girdle of quartz [0001]-axes is illustrated in Fig. 40. Although concentration is weak, two maxima and submaxima distribute symmetrically inside of *ac*-plane and on a small circle with angular radius 60° from fabric axis *b*. The pattern shows an orthorhombic symmetry.

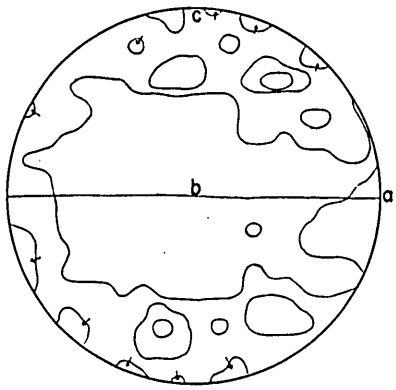

Fig. 40. Orientation diagram for [0001] in quartz in specimen 11 (pelitic schist), 500 grains. Contours: 3-2-1%.

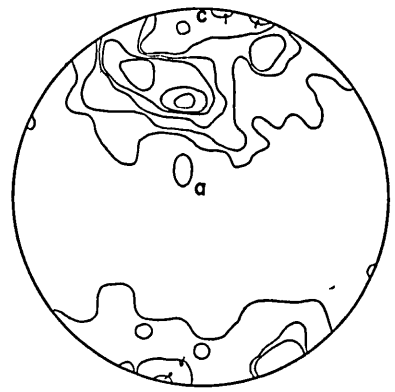

Fig. 41 Orientation diagram for [0001] in quartz in specimen 12 (spotted siliceous schist), 400 grains. Contours: 6-5-4-3-2-1%.

Specimen 12. (N058V27-3)

Siliceous schist, 250m south of the mining office of the Sazare mine. The locality is stratigraphically situated 150m upper than specimen 9 and structurally on the south limb of the anticline. It belongs to the zone IIa of the mineral zoning. The surface S_1 is distinct. The lineation L_1 and L_3 are mutually parallel and nearly horizontal. Component minerals are quartz, albite, muscovite, chlorite and epidote. On thin section are observed sheared zones with 0.1-2mm parallel to S_1. Quartz is small in grain size and shows strong undulatory extiction.

The pattern of [0001]-axes illustrates a small circle girdle around the fabric axis *c* (Fig. 41) and maxima distribute on the small circle girdle.

Specimen 13. (N059I20-10)

Spotted pelitic schist, collected from the main adit (510m from the entrance). The locality is stratigraphically situated 300m upper than specimen 10 and structurally on the south limb of the Yakushi anticline. It belongs to the zone IIa. The surface S_1 is distinctand cleavage S_{2-2} is observed on a thin section. The lineation L_1 is clear on S_1. Micro-scale folds of the type I are recognized on the section parallel to L_3 but not observed on one normal to L_3. Therefore, L_1 is nearly normal to L_3. Component minerals are quartz, albite, muscovite, and chlorite.

The orientation pattern of muscovite {001}-poles shows a strong maximum, hav-

ing a orthorhombic symmetry (Fig. 42a). In this specimen, preferred orientation of quartz lattice is weak. Three maxima distribute asymmetrically. Therefore, this pattern of the quartz diagram shows a triclinic symmetry (Fig. 42a).

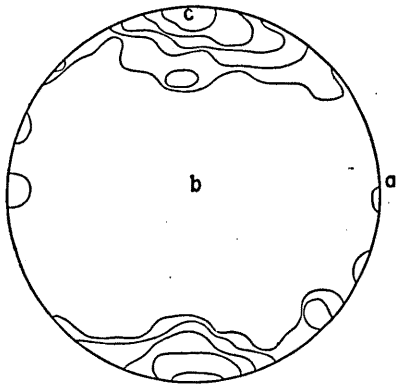

FIG. 42a Orientation diagram for {001} in chlorite and muscovite in specimen 13 (spotted pelitic schist), 100 grains. Contours: 15-10-5-1%.

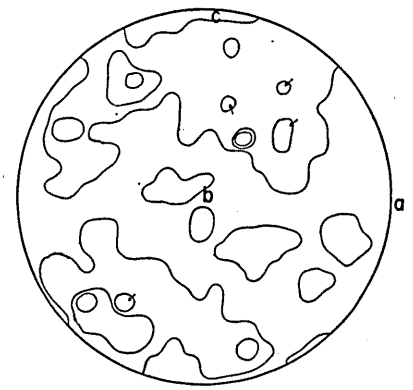

FIG. 42b Orientation diagram for [0001] in quartz in specimen 13 (spotted pelitie schist), 500 grains. Contours: 3-2-1%.

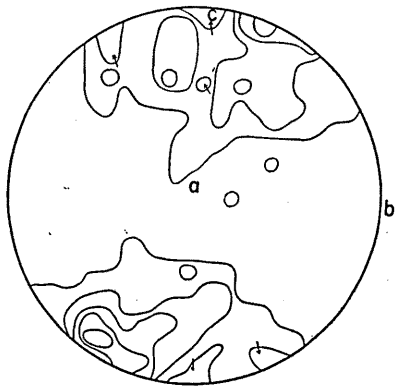

FIG. 43 Orientation diagram for [0001] in quartz in specimen 14 (spotted siliceous schist), 400 grains. Contours: 5-4-3-2-1%.

Specimen 14. (N059IX28-1)

Spotted siliceous schist, east of the Kinsha ore body on the 6th sublevel. The locality is situated on the upper horizon of the ore beds and in the zone IIb. The surface S_1 is distinct. Transversal schistosity-surfaces, (*h0l*) and (*0kl*), are weakly recognized. Component minerals are quartz, albite, muscovite, chlorite, epidote, colourless amphibole, and hematite.

In Fig. 43, a maximum and submaxima distribute near but not on *ac*-plane. The pattern of the quartz diagram is triclinic.

Specimen 15. (N058VI4-1)

Spotted siliceous schist, collected from the Kinsha ore body on the 6th sublevel. The locality is the same horizon as the specimen 14. The surface S_1 is distinct and the trantversal schistosity-surfaces are weak. The lineation L_1 is distinct and lineation normal to L_1 is observed. Component minerals are quartz, albite, muscovite, chlorite, epidote, bluish-green amphibole, and calcite. Quartz shows strong undulatory extinction and granulation in some layers.

Fig. 44a illustrates muscovite {001}-diagram on a *b*-section. It shows monoclinic

symmetry. In Fig. 44b, the pattern of quarts [0001]-axes lacks *ac*-girdle and is somewhat similar to that of specimen 14 (Fig. 43). Because of asymmetric distribution of maxima and submaxima, the quartz diagram has a triclinic symmetry.

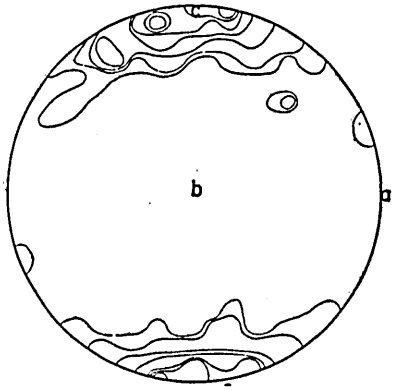

Fig. 44a Orientation diagram for {001} in muscovite and chlorite in specimen 15 (spotted siliceous schist), 200 grains. Contours: 11-10 -8-6-4-2-1%.

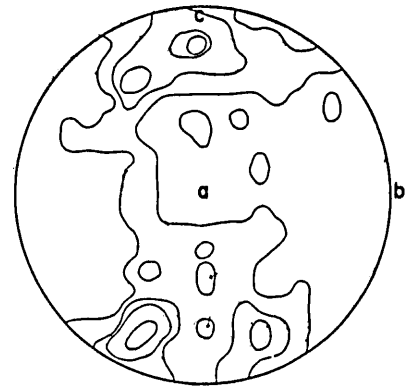

Fig. 44b Orientation diagram for [0001] in quartz in specimen 15 (spotted siliceous schist), 500 grain. Contours: 4-3-2-1%.

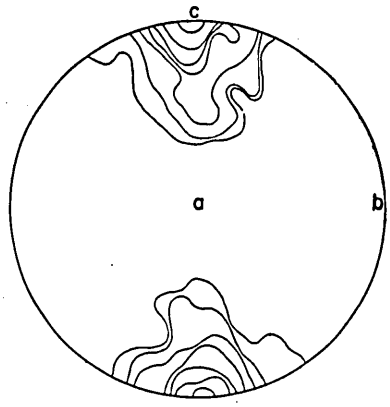

Fig. 45a Orientation diagram for {001} in muscovite and chlorite in specimen 16 (spotted siliceous schist), 200 grains. Contours: 15-10 -8-6-4-2-1%.

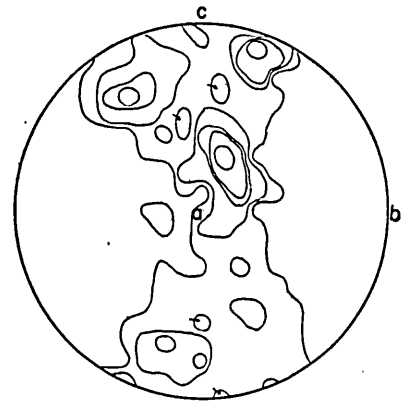

Fig. 45b Orientation diagram for [0001] in quartz in specimen 16 (spotted siliceous schist), 400 grains. Contours: 5-4-3-2-1%.

Specimen 16. (N058IX9-10)

Spotted siliceous schist, collected from the Shimpi ore body. The locality is the same horizon as the specimen 14 and 15. The surface S_1 is distinct. The conjugate sets of transversal schistosity-surface are developed. The lineation L_1 is distinct. L_3 is clear and normal to L_1. The lineation which is the intersection of S_1 and the conjugate sets of transversal schistosity surfaces is parallel to L_1 and may belong to L_2. Component minerals are quartz, albite, muscovite, chlorite, epidote, tourmaline and magnentite. Quartz grains show strong undulatory extinction and granulation in shear zones.

The pattern of muscovite {001}-pole diagram illustrates an orthorhombic symmetry (Fig. 45a). In quartz diagram, the symmetry is triclinic as judged from the

distribution of a maximum (Fig. 45b).

Specimen 17. (N058IX15-4)

Spotted siliceous schisst, collected from the Kinsha ore body on the 12th level. Stratigraphical position, structural position and mineralogical zone are equivalent to the specimen 14. The surface S_1 is distinct, but any transevrsal schistosity surface are not observed. The lineation L_1 is recognized on S_1. Component minerals are quartz, albite, muscovite and epidote. Quartz is equidimensional and shows weak undulatory extinction.

In Fig. 46, *ac*-girdle is not developed but maxima of quartz [0001]-axes distribute on a small circle around the fabric axis *c*. The symmetry of quartz diagram can be regarded as orthorhombic.

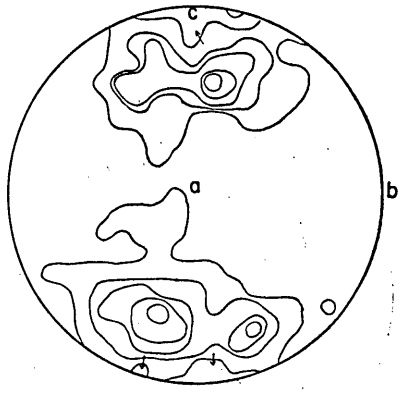

FIG. 46 Orientation diagram for [0001] in quartz in specimen 17 (spotted siliceous schist). Contours: 5-4-3-2-1%.

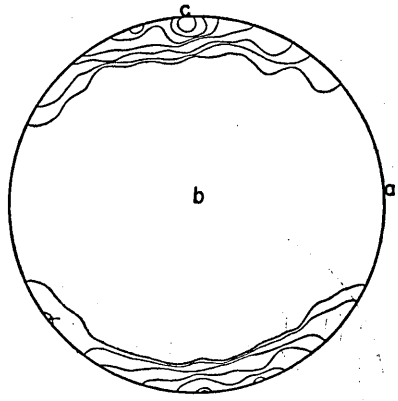

FIG. 47a Orientation diagram for {001} in muscovite in specimen 18 (spotted siliceous schist), 200 grains. Contours: 20-16-12-8-4-2-1%.

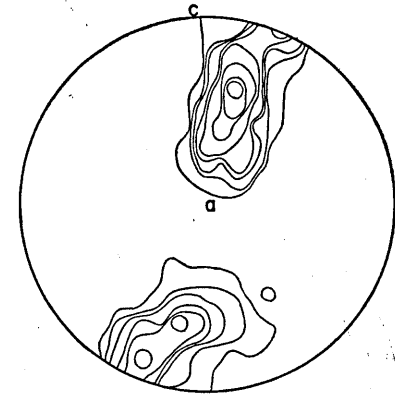

FIG. 47b Orientation diagram for [0001] in quartz in specimen 18 (spotted siliceous schist), 400 grains. Contours: 11-9-7-5-4-3-2-1%.

Specimen 18. (N058VIII28-3)

Siliceous schist, collected from the Tomisatomuke prospecting gallery on the 12th level. The locality is situated on the same horizon as the specimen 14 and structurally on the east part of the Tomisato fold. It belongs to the zone IIb. The surface S_1 is distinct but other schistosity surfaces are ralely observed. The lineation L_1 is distinct. Component minerals are quartz, albite, muscovite, chlorite, epidote, colourless amphibole, and garnet. Quartz shows elongated dimension oblqiue to S_1 and shows undulatory extinction.

In orientation diagram for {001} of muscovite, fabric pattern shows monocline symmetry (Fig. 47a). The pattern of the quartz diagram, however, has a triclinic symmetry (Fig. 47b).

Specimen 19. (N058IX18-7)

Spotted pelitic schist, collected from the main adit (860m from the entrance). The locality is situated 120m upper from the ore beds, and structurally on the south limb of the Yakushi anticline. It belongs to the zone IIb. The surface S_1 is distinct, but transversal schistosity-surfaces art not observed. The type I folds on a micro-scale are observed on the section and their axes are parallel to L_1. Component minerals are quartz, albite, muscovite, chlorite, graphite, and tourmaline.

In muscovite, pattern of {001} pole diagram shows a maximum and illustrates orthorhombic symmetry (Fig. 48a). In quartz diagram (Fig. 48b), a maximum and a submaximum distribute asymmetrically and fall on a small circle around the fabric axis *c*. The symmetry of the diagram is triclinic.

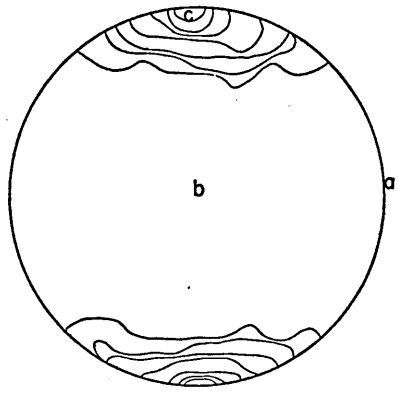

FIG. 48a Orientation diagram for {001} muscovite and chlorite in specimen 19 (spotted pelitic schist), 200 grains. Contours: 19-16-12-8-4-2-1%.

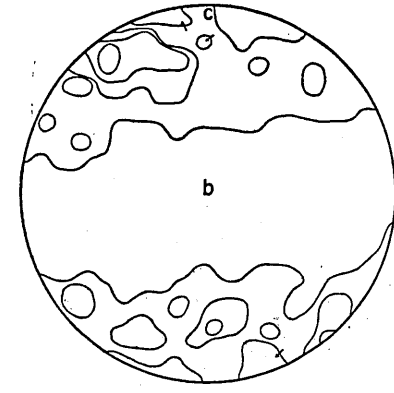

FIG. 48b Orientation diagram for [0001] in quartz in specimen 19 (spotted pelitic rchist), 500 grains. Contours: 4-3-2-1%.

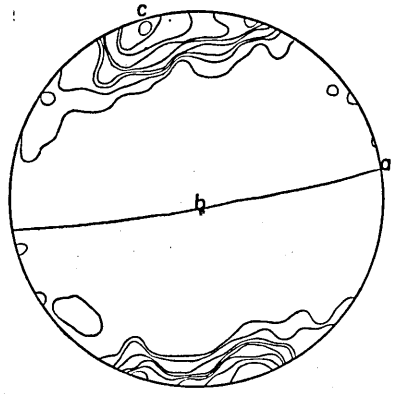

FIG. 49a Orientation diagram for {001} in muscovite in spcimen 20 (speotted siliceous schist), 200 grains. Contours: 15-12-10-7-5-4-3-2-1%.

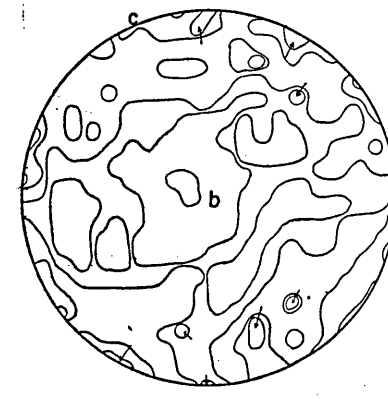

FIG. 49b Orientation diagram for [0001] in quartz in specimen 20 (spotted siliceous schist), 500 grains. Contours: 3-2-1%.

Specimen 20. (N058V27-7)

Siliceous schist, collected from 850m south of the mining office. The locality is situated 160m upper from the ore beds (the Upper member of the Minawa formation) and structurally on the south limb of the Yakushi anticline. It belongs to the zone IIb. The turface S_1 is distinct, but other schistosity surfaces are not recognized. The lineation L_1 is weak and the lineations oblique to L_1 are slightly recognized. The type I fold on a small scale is recognized in the specimen. Component minerals are quartz, albite, muscovite, chlorite, and glaucophanic amphibole. Quartz grains show undulatory extiction but not granulation.

The orientation diagram for {001} of muscovite shows a monoclinic symmetry (Fig. 49a). In the quartz [0001]-axes diagram, an incomplete girdle on *ac*-plane is recognized (Fig. 49b).

Although concentration is weak, the symmetry of the pattern may be triclinic.

In the preceding pages, orientation data for [0001] of quartz and for {001} of mica and chlorite have been described from various localities from the lower horizon to the upper horizon (from the zone I to the zone IIb).

Mica and chlorite fabrics show no essential differences in orientation pattern in the area concerned. On each mica and chlorite diagram, a partial girdle on *ac*-plane is clearly developed. A distinct maximum with high concentration falls on *ac*-girdle and coincides with the fabric axis *c*. Therefore, it is normal to S_1. The symmetry of mica and chlorite fabrics is generally orthorhombic in some specimens monoclinic. While, in quartz diagrams, there can be recognized four types of orientation pattern as follows: 1) the fabric pattern with *ac*-girdle on which maxima and submaxima distribute, 2) the fabric pattern with a small circle with angular radius 60°～70° and with maxima and submaxima somewhat apart from *ac*-plane, 3) the fabric pattern with a small circle girdle with angular radius 20°～30° on which maxima and submaxima distribute, and 4) the fabric pattern with a strong maximum on ill developed girdle.

Many quartz diagrams which belong to the types 1), 2) and 3) show nearly orthorhombic symmetry. However, if positions of maxima and submaxima are strictly considered, those fabric patterns of quartz diagrams may be triclinic (specimens 10, 12, 13, 14, 15, 16 and 19). In quartz diagrams with orthorhombic symmetry (specimens 9, 10 and 17), intersections of symmetry planes are parallel to the lineation L_1 or B_1, it may not necessarily indicate that present quartz fabrics were imprinted during the stage of the type I folds. In many cases, L_2 and B_2 are nearly parallel to L_1 and B_1. In some places of the zone IIb, L_3 is nearly normal to L_1 or L_2. These geometric relations may reflect on the quartz fabric, if the formation of it was during the stages of deformation related to the formation of L_2 and L_3. In specimen 18 which is collected from the core of the Tomisato fold, the quartz fabric shows a distinct triclinic symmetry with strong maxima. As discussed in chapter IV and V, the Tomisato fold is characterized by the type II folds. From this point, some of quartz fabrics may be formed also by the type II folds.

Quartz [0001]-fabrics have been interpreted in terms of gliding of certain glide systems in quartz on slip planes in tectonites by many authors. This interpretation,

however, has not been tested by preferred orientation of any crystallographic line or plane other than [0001]. Stable orientations of minerals under nonhydrostatic stress have been discussed by KAMB (1959, 1961) and BRACE (1960), but with no consistent results, and their theories and predicted state of orientation were not successfully compared with natural and experimentally induced fabrics. TURNER and WEISS (1963) said, "the significant property of a quartz pattern is its symmetry", in the present state of knowledge regarding the mechanics of the orientation of quartz. From the symmetry of quartz pattern, they introduced dynamic interpretation as follows: in orthorhombic symmetry, "the three mutually perpendicular directions of intersection of the planes of near-symmetry could be equated with the axes of principal stress σ_1, σ_2, and σ_3". And they considered, "the axis of the stress system lies somewhere in the plane of the girdle". Then in the present definition of the fabric axes, σ_1 could be equated with fabric *a*- or *c*-axis and σ_2 or σ_3 could be equated with *b*-axis. On the basis of correlation between the symmetry of calcite fabrics and that of quartz fabrics, the stress system for some types of quartz fabrics was discussed and established by HARA (1961, 1962). From the fabric pattern of the type 2) and 3), stress systems could be inferred on the basis cited above. In the type 3), the fabric axis *c* which is the centre of a small circle girdle with radius 20°~40° could be equated σ_1. In the type 2), the fabric axis *b* which is the pole of *ac*-girdle or the centre of a small circle girdle with radius 60°~70° could be equated to σ_3. Therefore, it can be inferred as a probable dynamic interpretation that rocks of the present area were subjected to the maximum compression normal to S_1 or maximum tension parallel to b ($=L_1$) during the stage of development of quartz [0001] fabrics.

C. PETROFABRIC ANALYSIS OF SMALL-SCALE FOLDS

1. *Type I folds.*

Specimen 21. (N0581IX17-3)

Spotted siliceous schist, collected from the Kinsha ore body on the 19th level of the Sazare mine. The type I folds on a small scale are developed at locality. The specimen includes one of these folds. Schistosity-surface S_1 is recognized as compositional banding which is composed of epidote-amphibole-rich layers and quartz-rich layers.

In muscovite grains, undulatory extinction is lacking or weak and bending of basal cleavages can not be recognized. In Fig. 50, {001}-poles of muscovite and [0001] of quartz were measured in quartzose layer in each sector. In muscovite, patterns of diagrams are similar in each sectors (cf. Fig. 50b~e). Therefore, muscovite fabric may regarded as homogeneous in the analysed domain. In these diagrams, {001}-poles fall on *ac*-girdle and hardly normal to S_1 but nearly normal to axial surface of the fold. Therefore, basal cleavages of large numbers of muscovite grains tend to orient parallel to the axial surface with tendency of fan-like distribution. Small numbers of them are oriented parallel to S_1.

In this specimen, quartz grains are large and equant in grain size. They are slightly elongated parallel to the axial surface of the fold near the hinge zone. They show sharp grain boundary and are lacking in grain boundary granulation. Quartz

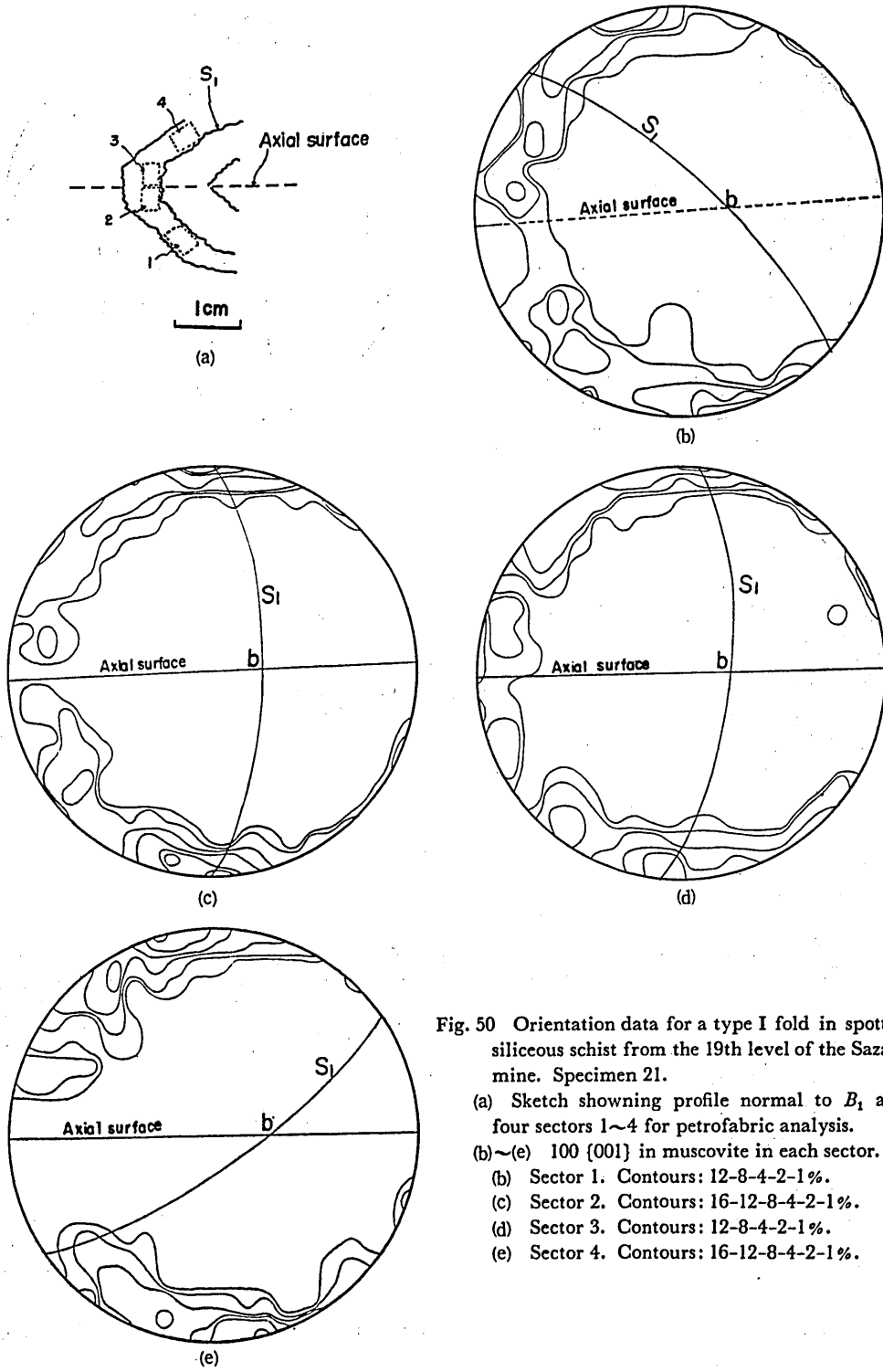

Fig. 50 Orientation data for a type I fold in spotted siliceous schist from the 19th level of the Sazare mine. Specimen 21.

(a) Sketch showning profile normal to B_1 and four sectors 1~4 for petrofabric analysis.

(b)~(e) 100 {001} in muscovite in each sector.

(b) Sector 1. Contours: 12-8-4-2-1%.

(c) Sector 2. Contours: 16-12-8-4-2-1%.

(d) Sector 3. Contours: 12-8-4-2-1%.

(e) Sector 4. Contours: 16-12-8-4-2-1%.

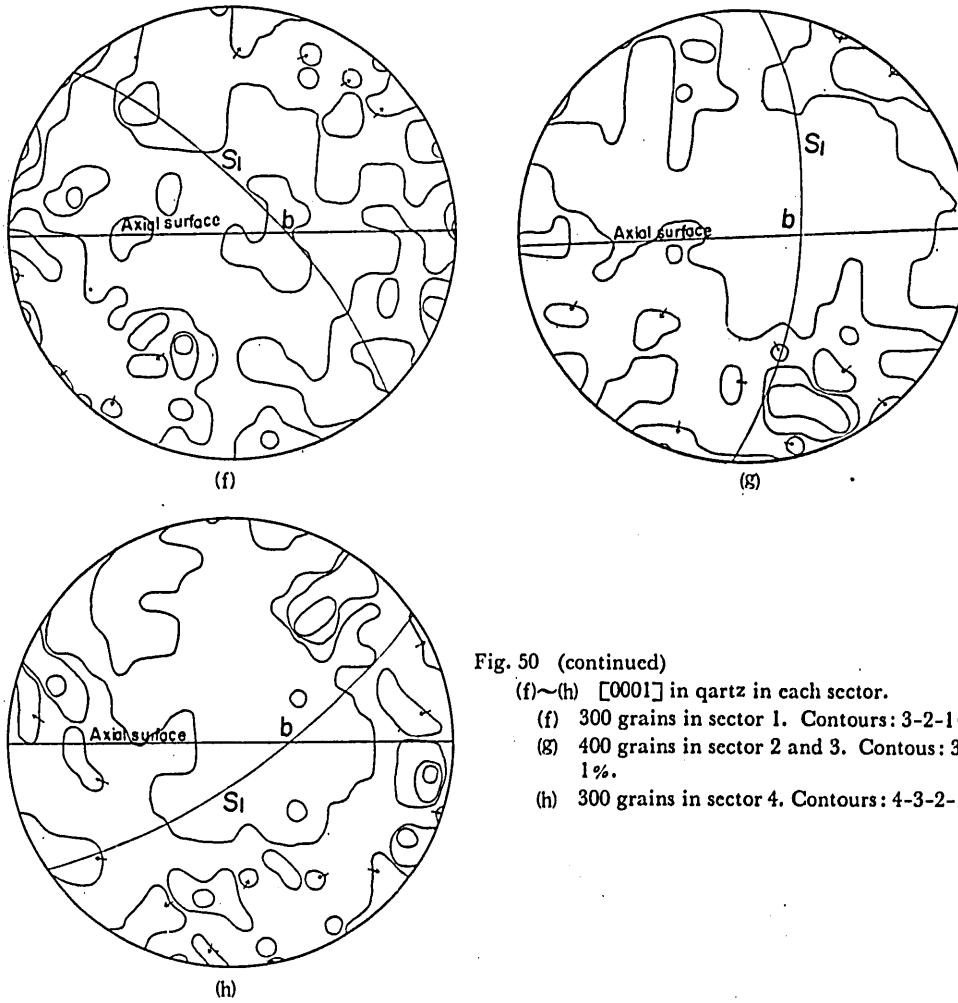

Fig. 50 (continued)
(f)~(h) [0001] in qartz in each sector.
(f) 300 grains in sector 1. Contours: 3-2-1%.
(g) 400 grains in sector 2 and 3. Contous: 3-2-1%.
(h) 300 grains in sector 4. Contours: 4-3-2-1%.

[0001]-axes are measured in three sectors as shown in Fig. 50f~h. Although concentration of quartz [0001]-axes is weak, an incomplete girdle is recognized in each diagram. However, positions of maxima in one sector can not be correlated with those in other sectors. Maxima with low concentration distribute inside the *ac*-girdle (approximately 10° to 30° from *ac*-plane) in any sectors. Therefore, it can be regarded that quartz fabrics are practically homogeneous through these sectors with respect to distribution range of maxima.

Specimen 8. (N061VIII31-1)

Piedmontite bearing siliceous schist, collected from the east side of the Dozan River. The specimen is the same as described for piedmontite fabric. A fold of the type I on a small scale is observed in this specimen. Quartzose layers are generally thicker in the hinge zone than on the limb of the fold. Muscovite and chlorite shows weak undulatory extinction.

On the limb of the fold, a maximum for {001} poles in chlorite is normal to S_1,

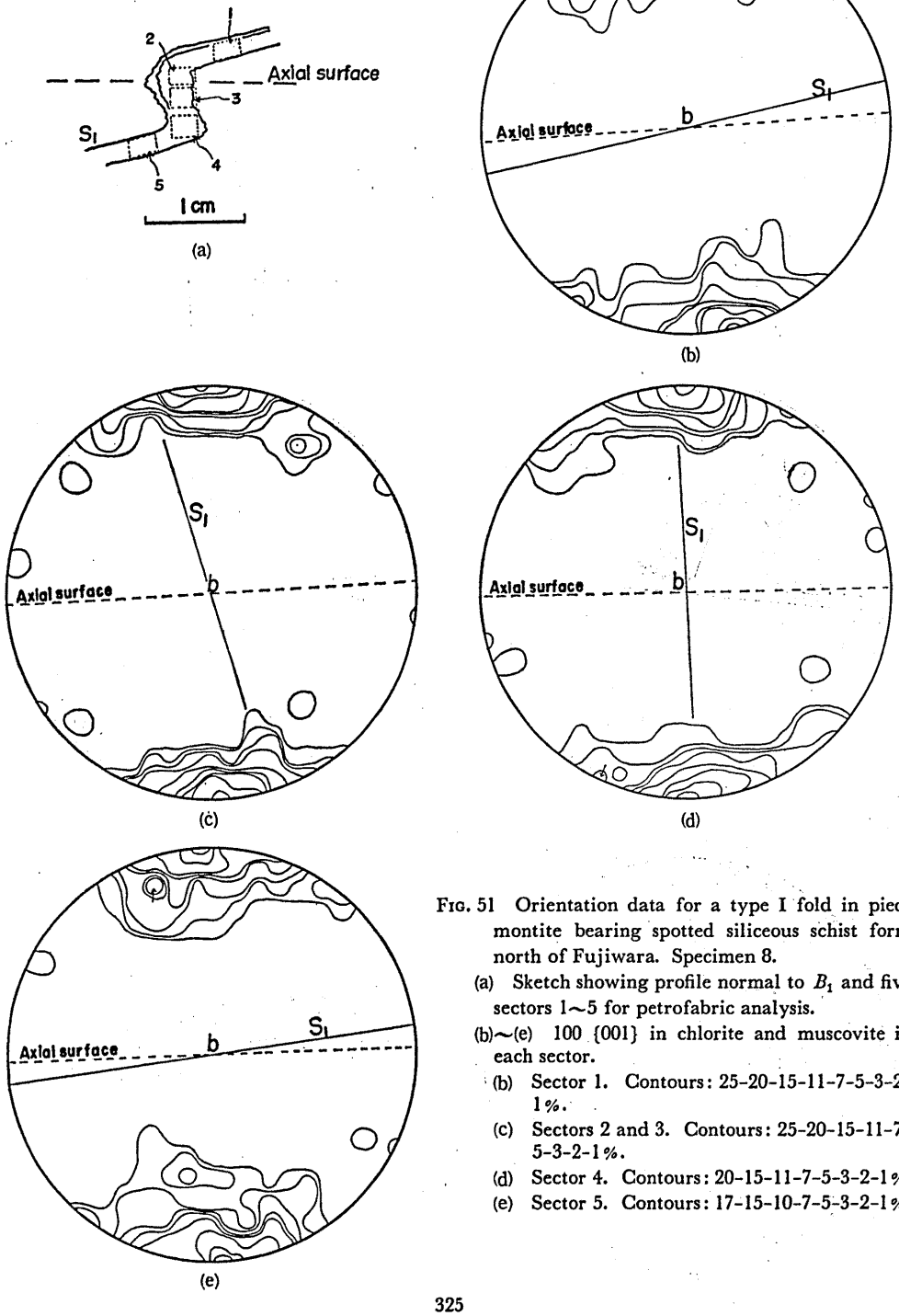

FIG. 51 Orientation data for a type I fold in piedmontite bearing spotted siliceous schist form north of Fujiwara. Specimen 8.

(a) Sketch showing profile normal to B_1 and five sectors 1~5 for petrofabric analysis.

(b)~(e) 100 {001} in chlorite and muscovite in each sector.

(b) Sector 1. Contours: 25-20-15-11-7-5-3-2-1%.

(c) Sectors 2 and 3. Contours: 25-20-15-11-7-5-3-2-1%.

(d) Sector 4. Contours: 20-15-11-7-5-3-2-1%.

(e) Sector 5. Contours: 17-15-10-7-5-3-2-1%.

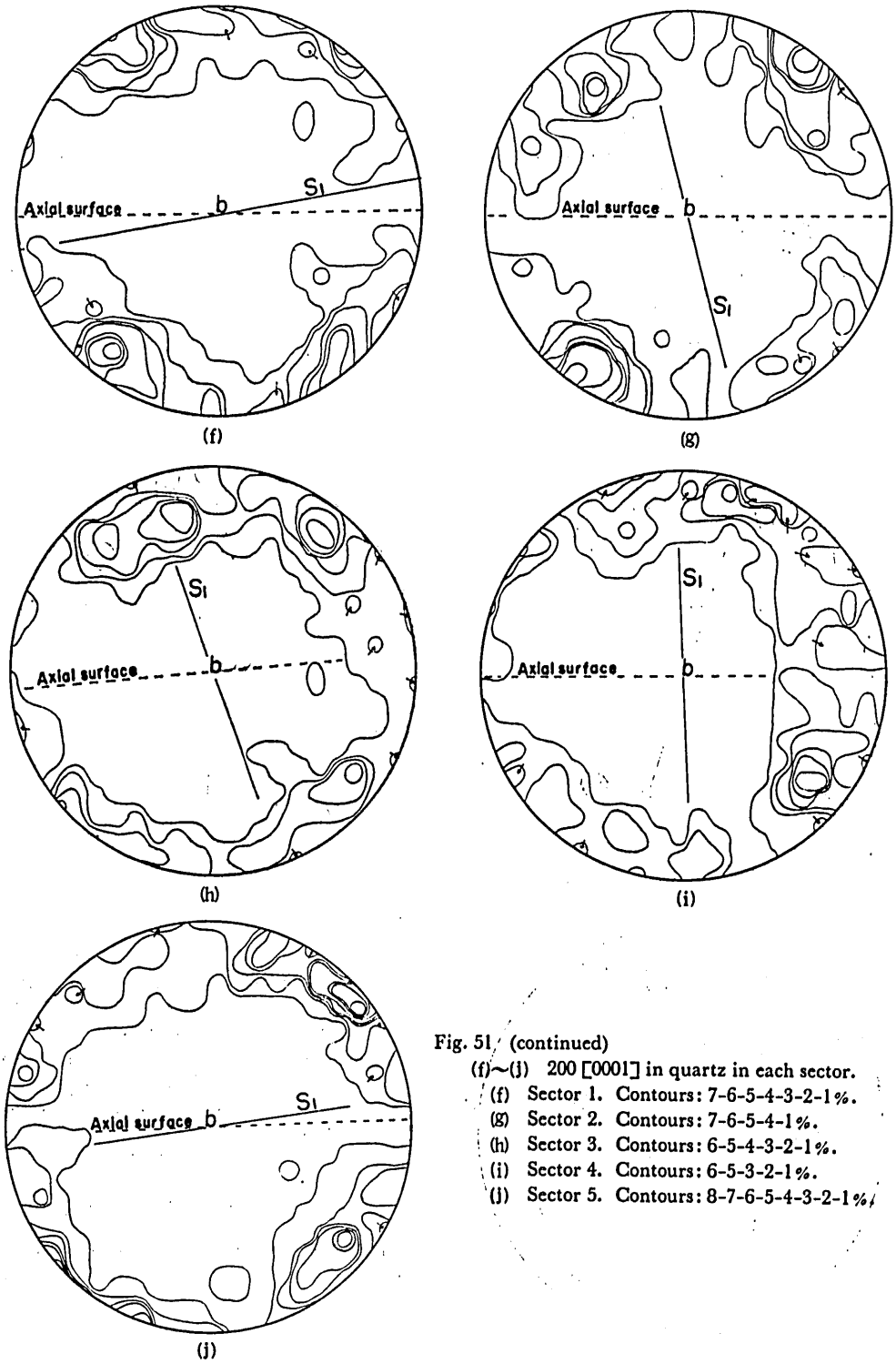

Fig. 51 (continued)

(f)~(j) 200 [0001] in quartz in each sector.

(f) Sector 1. Contours: 7-6-5-4-3-2-1%.
(g) Sector 2. Contours: 7-6-5-4-1%.
(h) Sector 3. Contours: 6-5-4-3-2-1%.
(i) Sector 4. Contours: 6-5-3-2-1%.
(j) Sector 5. Contours: 8-7-6-5-4-3-2-1%.

but in the hinge it is normal to the axial surface of the fold (Fig. 51b~e). Therefore, tendency of preferred orientation of phyllosilicates is somewhat different between two specimens (8 and 21).

As already described in page 35, Y-axes of peidmontite are parallel to the fold axis (B_1) and X-axes are nearly normal to S_1. Z-axes are nearly normal to the fold axis on the axial surface. Therefore, $\{10\bar{2}\}$-poles are parallel to the axial surface in the hinge zone.

On a thin section normal to the fold axis (B_1), quartz grains are elongated with their long axis parallel to S_1 or axial surface of the fold. Undulatory extinction is strong.

Orientation pattern of [0001]-axes of quartz is approximately homogeneous through the fold (Fig. 51f~j). In four sectors (1, 2, 4 and 5), orientation pattern of [0001]-axes shows orthorhombic symmetry with three symmetry planes, parallel to *ac*-(periphery), to *ab*-, and to *bc*-planes. In the sector 3, a submaximum near the fabric axis *c* reduces symmetry of orientation diagrams from orthorhombic to triclinic, but the pattern is approximately equal to that of other sectors. Symmetry of quartz fabric coincides practically with that of muscovite and chlorite.

2. *Type III fold.*

Specimen 22. (N059VIII29-8)

Spotted pelitic schist, 1100m north of Fujiwara. The locality is situated stratigraphically in the Upper member of the Minawa formation, and structurally on the north limb of the Tsuneyama syncline. It belongs to the zone III of mineral zoning. Schistosity-surface S_1 is distinct and S_1 is folded by the type III folds on a small scale. In the hinge zone, cleavage S_{2-2} is developed. Lineation L_3 is distinct on S_1 and weak striations normal to L_3 are recognized on S_1. Component minerals are quartz, albite, muscovite, chlorite, tourmaline and opaque materials (graphite). Muscovite and chlorite are bent around micro-scale fold axes of the type III folds or S_{2-2}-surfaces.

Three sectors are set up in a quartz-albite-muscovite layer around the hinge of the fold, as shown in Fig. 52a. Fig. 52b~d illustrate orientation data of {001}-axes for muscovite. In the hinge of the fold (sector 2), {001}-axes for muscovite is oriented parallel to S_1 and hardly to S_{2-2}. Although the angle between two limbs of the fold (sectors 1 and 3) is only 37°, a maximum of muscovite {001}-axes in each diagram is normal to S_1. Therefore basal cleavage of muscovite are parallel to S_1.

VII. Concluding Remarks

Structural development of the Sambagawa crystalline schists of the Sazare district as discussed in preceding chapters is summarized in the Table 2.

The axis of the type I fold is defined as B_1 (see page 16). During the folding of the type I, original bedding surface was transposed towards the axial surface of the type I fold which is almost parallel to the gross lithologic layering. Basal cleavage plane of mica and chlorite, {100} of amphiboles and in some cases $\{10\bar{2}\}$ of epidote are parallel to the axial surface (see pages 29 and 31). *c*-Axis of amphiboles and *b*-axis of epidotes are parallel to the fold axis (B_1). Although there are many prob-

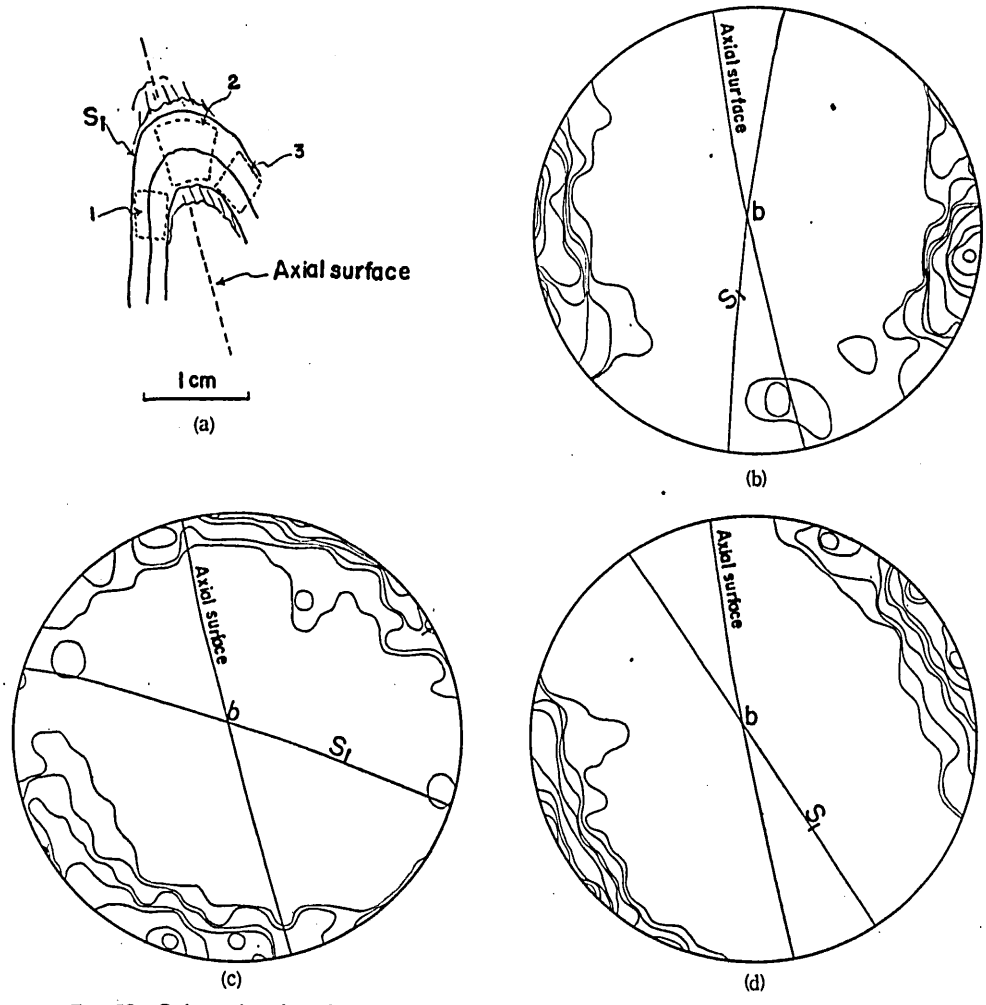

Fig. 52 Orientation data for a tpye III fold in spotted schist from norh fo Fujiwara.
(a) Sketch showing profile normal to B_3 and three sectors 1~3 for petrofabric analysis.
(b)~(d) 100 {001} in muscovite in each sector.
(b) Sector 1. Contours: 12-10-8-6-5-3-2-1%.
(c) Sector 2. Contours: 8-6-5-4-3-2-1%.
(d) Sector 3. Contours: 10-8-6-5-4-3-2-1%.

lems unsolved concerning the mechanics of preferred orientation of these minerals, strong orientation of these main component minerals in the metamorphic rocks suggests that the type I fold was synchronous with metamorphism. The related linear structures to the type I fold are L_1 and L_m (see page 16). The trend of B_1, L_1, and L_m is variable throughout the district, especially in the upper horizons: from the Upper member of the Minawa formation to the Ojoin formation (see pages 18 and 23). During the deformation related to the type I fold, the kinematic axis was heterogeneously oriented in this district, especially in the upper horizons. It suggests

TABLE 2. STRUCTURAL DEVELOPMENT OF THE SAMBAGAWA CRYSTALLINE SCHISTS OF THE SAZARE MINING DISTRICT.

	Time ⟶			
Planar atructures	Bedding S_1 $\begin{cases} s_1 \\ s_2 \\ s_m \end{cases}$	$\overbrace{S_{2-1} \quad S_{2-2}}^{S_2}$		
Types of folds	Type I	Type II	$\begin{cases} \text{Type III} \\ \text{Type IV} \end{cases}$	Type V
B-axes	B_1	B_2	B_3	B_4
Linear structures	$\begin{cases} L_1\ (=s_1 \wedge s_2) \\ L_m \end{cases}$	$L_2\ (=S_1 \wedge S_{2-1})$	$\begin{cases} L_3\ (=S_1 \wedge S_{2-2}) \\ L_4\ (=S_{2-1} \wedge S_{2-2}) \end{cases}$	L_5

that the stress plan related to the type I fold was also heterogeneous in this district.

B_1, L_1, and L_m are refolded by the type II fold. The axis of the type II fold which is designated as B_2 (see page 17) is sometimes nearly parallel to that of the type I fold. Transposition of S_1 towards the axial surface is also observed in the type II fold but weaker than in the type I fold. Preferred orientation of metamorphic minerals such as mica, chlorite, and amphiboles is less controled by the axial surface of the type II fold than by that of the type I fold. These minerals often show polygonal texure around the hinge of the type II fold, that suggesting annealing recrystallization after the type II folding. The orientation of B_2 and L_2 is also variable throughout the district. It suggests that movement plan and stress plan were also heterogeneous in this district during the deformation related to the type II fold.

Some fold form (s_i) in porphyroblasts of albitic plagioclase is identified to the type II fold. Therefore, some grains of albite porphyroblasts must have crystallized after this type of folding.

The type II fold is refolded by the type III and IV folds which are characterized by combination of concentric folding and strain-slip or fracture cleavage. In these types of folds, transposition of S_1 is very weak and orientation of mica and chlorite is hardly controled by the axial surface of the fold. Metamorphic minerals such as mica, chlorite, and amphiboles are bent. This texture suggests that crystallization of these main constituent mafic minerals were completed before the deformation related to the type III and IV folds. Strike of cleavage surface S_{2-2}, trend of B_3 (page 17), and axes of the type III and IV folds are fairly constant throughout the district as discussed in pages 18 and 25. In other words, kinematic axis b was homogeneous throughout the district during the phase of deformation related to these types of folds. It suggests that the stress plan was fairly homogeneous throughout the district concerned during the deformation related to these structures.

Small difference between the trend of B_3 and that of the axis of the Yakushi anticline is recognized. It suggests that the formation of the Yakushi anticline does not simply correspond to the deformation related to L_3, L_4, and B_3.

The "hinouchi-lineation (ore zone lineation)" or "*a*-lineation" by Takeda (1954), the "abnormal lineation" by Horikoshi (1958), "L_2-lineation" by Hirata (1959) and Doi (1959) are identical with linear structures L_1, B_1, L_2, and B_2 in the sense of the present author. Therefore, these linear structures are older than L_3, L_4, and B_3.

References

Banno, S. (1959) : Aegirineaugite from crystalline schists in Shikoku. *Jour. Geol. Soc. Japan*, **65**, 652-657.

Brace, W., F. (1960) : Orientation of Anisotropic Minerals in a Stress Field: Discussion. *Rock Deformation. Geol. Soc. Am. Memoir* **79**, 9-20.

Doi, M. (1959) : Geology and ore deposits of the Sazare Mine, Ehime prefecture, Japan (in Japanese). *Jour. Soc. Min. Geol. Japan* **9**, (35), 137-149.

——— (1961) : Geology and cupriferous pyrite deposits (Besshi type) of the Sanbagawa metamorphic zone including the Besshi and the Sazare Mine in central Shikoku (I) (in Japanese). *Jour. Soc. Min. Geol. Japan*, **11**, (50), 610-625.

Hara, I. (1961) : Dynamic interpretation of the simple type of calcite and quartz fabrics in the naturally deformed calcite-quartz vein. *Jour. Sci. Hiroshima Univ., Ser. C*, **4**, (1), 35-54.

——— (1962) : Studies on the structure of the Ryoke metamorphic rocks of the Kasagi district, Southwest Japen. *Jour. Sci. Hiroshima Univ., Ser. C*, **4**, (2), 163-224.

Hide, K. (1954) : Geological structure of the Sazare mining district, Kochi prefecture. *Geol. Rep. Hiroshima Univ.*, (4), 45-82.

Hide, K., Yoshino, G., and Kojima, G. (1956): Preliminary report on the geologic structure of the Besshi spotted schist zone (in Japanese). *Jour. Geol. Soc. Japan*, **62**, 574-584.

Hide, K. (1961) : Geologic structure and metamorphism of the Sambagawa crystalline schists of the Besshi-Shirataki mining district in Shikoku, Southwest Japan (in Japanese). *Geol. Rep. Hiroshima Univ.*, (9), 87.

Hirata, Y. (1959) : Geology and ore deposits in the Sazare mining district (abstract in Japanese). *Jour. Geol. Soc. Japan*, **66**. 421.

Horikoshi, E. (1958) : The lineation and the ore bodies of the Sazare mine (in Japanese). *Jour. Soc. Min. Geol. Japan*, **8**, (1), 33-40.

Ishioka, K. and Suwa, K. (1954) : Fabric of hornblende in schistose amphibolite from the Kurobe-gawa area, central Japan. *Jour. Earth Sci. Nagaya Univ.* **2**, (2), 191-199.

Iwasaki, M. (1960a) : Colourless glaucophane and associated minerals in quartzose schists from eastern Shikoku, Japan. *Jour. Geol. Soc. Japan*, **66**, 566-574.

——— (1960b) : Barroisitic amphibole from Bizan in eastern Shikoku, Japan. *Jour. Geol. Soc. Japan*, **66**, 625-630.

——— (1963) : Metamorphic rocks of the Kotu-Bizan Area, Eastern Shikoku. *Jour. Fac. Sci. Tokyo Univ., Sec. II*, **15**, (1), 1-90.

Johnson, M. R. W. (1956) : Conjugate fold systems in the Moine thrust zone in the Lochcarron and Coulin Forest area of Wester Ross. *Geol. Mag.*, **93**, 345-350.

Kamb, W. F. (1959) : Theory of the preferred crystal orientation developed by crystallization under stress. *Jour. Geol.*, **67**, (2), 153-170.

Knill, J. L. (1960) : A classification of cleavages, with special reperences to the Craignish district of the Scottish Highlands. *Report of the Twentyfirst seccion, Intern. Geol. Congr., Part* **18**, 317-325.

Kojima, G. (1951a) : Über das "Feld der Metamorphose" der Sanbagawa Kristallinen Schiefer-besonders in Bezug auf Bildung der Kristallinen Schiesergebietes in Zentral-Shikoku. *Jour. Sci. Hiroshima Univ., Sec. C*, **1**, (1), 1-18.

——— (1951b) : Stratigraphy and geological structure of the crystalline schist region in Central Shikoku (in Japanese). *Jour. Geol. Soc. Japan*, **57**, 177-190.

Kojima, G., Hide, K. and Yoshino, G. (1956) : The stratigraphical position of Kieslager in the Sambagawa crystalline schist zone in Shikoku (in Japanese). *Jour. Geol. Soc. Japan*, **62**, 39-45.

KOJIMA, G. and HIDE, K. (1957) : On new occurrence of aegirine augirine augite-amphibole-quartz-schists in the Sambagawa crystalline schists of the Besshi-Shirataki district, with special reference to the preferred orientation of aegirine augite and amphibole. *Jour. Sci. Hiroshima Univ., Ser. C*, **2**, (1), 1-20.

——— (1958) : Kinematic interpretation of the quartz fabric of triclinic tectonites from Besshi, Central Shikoku, Japan. *Jour. Sci. Hiroshima Univ., Ser. C*, **2**, (2), 195-226.

KOJIMA, G. and SUZUKI, T. (1958) : Rock structure and quartz fabric in a thrusting sheared zone: the Kiyomizu tectonic zone in Shikoku, Japan. *Jour. Sci. Hiroshima Univ., Ser. C*, **2**, (3), 173-194.

LADURNER, J. (1951) : Deformation Wachstum und Regelung der Epidote als Gefügekorn und Einkristall. *Tschermaks Min. Petrol. Mitt.*, **82**, (3), 317-412.

LEITH, C. K. (1905) : Rock cleavage. *Geol. Surv. America Bull.*, (239).

MIYASHIRO, A. and BANNO, A. (1958) : Nature of glaucophanic metamorphism. *Amer. Jour. Sci.*, **256**, 97-110.

MIYASHIRO, A. (1959) : Abukuma, Ryoke, and Sanbagawa metamorphic belts (in Japanese). *Jour. Geol. Soc. Japan*, **65**, 624-637.

NAKAYAMA, I, (1953) : Stratigraphy and gecological structure of the Sanbagawa crystalline schist in the northern part of the Tenryu river district (in Japanese). *Jour. Geol. Soc. Japan*, **59**, 497-509.

——— (1954) : The relation of the lineation to the geological structure in the Sambagawa metamorphic zone of the Tenryu river basin. *Mem. Coll. Kyoto Univ., Ser., B*, **21**, 273-286.

——— (1960) : The tectonic movement and the rock structure of the Sambagawa metamorphic zone, Japan (in Japanese). *Monograph of the Assoc. Geol. Collaboration in Japan* (10).

ODA, K. (1961) : On the ore deposit and folding of the Sazare Mine (in Japanese). *Tansakoenshu (Lectures for Prospect)*, 101-107.

OGAWA, T. (1902) : Explanatory text of the geological map of Japan, scale 1 ; 200,000, Kochi.

OSHIMA, T., IWASAKI, M. and NAKAYAMA, I. (1963) : Geology and Petrography of the Vicinity of Kotu Mine, Eastern Shikoku (in Japanese). *Jour. Geol. Soc. Japan.* **69**, 243-251.

OYAGI, N. (1960) : "Abnormal lineation" in the Sazare Mine, Ehime prefecture (abstract in Japanese). *Jour. Geol. Soc. Japan*, **67**, 448.

——— (1963) : Preferred orientation of tourmaline in crystalline schists from the Sazare Mine, in central Shikoku, Japan. *Geol. Rep. Hiroshima Univ.*, (12), 493-502.

OZAWA, G. (1926) : Stratigraphy and strucuture of the crystalline schist system in Shikoku (in Japanese). *Jour. Geol. Soc. Japan*, **33**, 297-304, 309-329.

RAMSAY, J. G. (1960) : The deformation of early linear structures in Areas of repeated folding. *Jour. Geol.*, **68**, (1), 75-93.

PATERSON, M. S. and WEISS, L. (1961) : Symmetry concepts in the structural analysis of deformed rocks. *Geol. Soc. America bull.*, **72**, 841-882.

READ, H. H. (1949) : A contemplation of time in plutonism. *Quart. Jour. Geol. Soc. Lonbon*, **110**, 101-156.

SANDER, B. (1930) : *Gefügekunge der Gesteine.* Wien, Springer.

——— (1948) : *Einführung in die Gefügekinde der geologischen Körper. Ier Teil, Allgmemeine Gefügekunde und Arbeiten im Bereich Handstuck bis Profil.* Wien und Innsbruck.

——— (1950) : *Einführung in die Gefügekunde der geologischen Körper. IIer Teil, Die Korngefuge.* Wien und Innsbruck.

SATO, (1938) : Geological map of Japan, sale 1 : 75,000, Ni-ihama.

SEKI, Y. (1958) : Glaucophanic regional metamorphism in the Kanto Mountains, Central Japan. *Jap. Jour. Geograph. Geol.* **29**, (4), 233-258.

TAKEDA, H. (1954) : Geology and ore deposit of the Sazare Mining district (preliminary report) (in Japanese). *Geol. Rep. Hiroshima Univ.*, (4), 35-45.

TURNER, F. J. and VERHOOGEN, J. (1951) : *Igneous and Metamorphic Petrology.* New York McGraw-Hill.

TURNER, F. J. (1957) : Lineation, symmetry, and internal movement in monoclinic tectonite fabrics. *Bull. Geol. Soc. America.*, **68**, 1-18.

TURNER, F. J. and WEISS, L. E. (1963) : *Structural analysis of metamorphic tectonites.* New York, McGraw-Hill.

Weiss, L. E. and McIntyre, D. B. (1957) : Structural geometry of Dalradian rocks at Loch Leven. Scottish Higlands. *Jour. Geol.*, **65**, (6), 575-602.

Weiss, L. E. (1959) : Geometry of superposed folding. *Bull. Geol. Soc. America*, **70**, (1), 91-106.

Yoshino, G. and Kojima, G. (1953) : Geological structure of the Ehime Mining district, Ehime Prefecture (in Japanese). *Jour. Geol. Soc. Japan*, **59**, 424-434.

Yui, S. (1960) : Two directions of linear structures, fold axes and ore shoot found in the vicinity of the Motoyasu Mine, Ehime Prefecture (abstruct in Japanese). *Jour. Geol. Soc. Japan*, **66**, 447.

Zwart, H. J. (1960) : Relations between folding and metamorphism in the central Pyrenees, and their chronological succession. *Geol. Mijn.* 39e Jaargang, Nr 5, 163-180.

Explanation of Plate XXIX

Fig. 1 Style of type II folds in spotted pelitic schist at 1 km north of Fujiwara. White layers are quartzose layers and quartz veins. Axial surfacet are nearly horizontal. Azimuth of fold axes is N-S. This figure is looking southward.

Fig. 2 Style of type III folds in spotted pelitic schist at 200m west of Fujiwara. White layers are quartzose layers. Axial surfaces are nearly vertical or dip steeply to the south. Azimuth of these fold axes is WNW. This figure is looking to the west.

Fig. 3 Style of type III folds in spotted pelitic schist at 1 km north of Fujiwara. Axial surfaces dip steeply to the south. Fold axes plunge 5° to WNW. This figure is looking to the west.

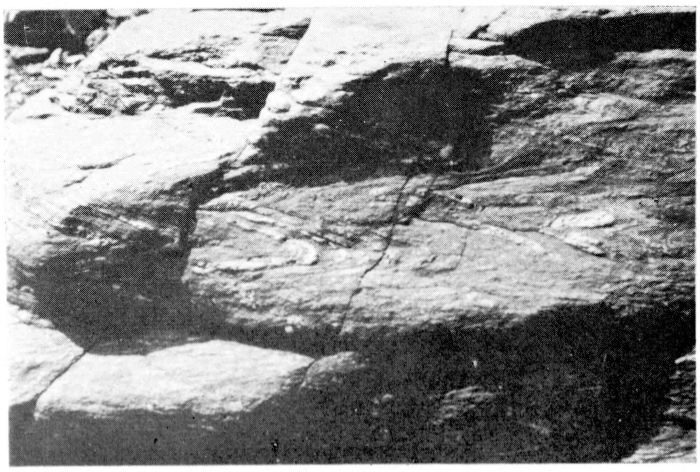

FIG. 1

FIG. 2

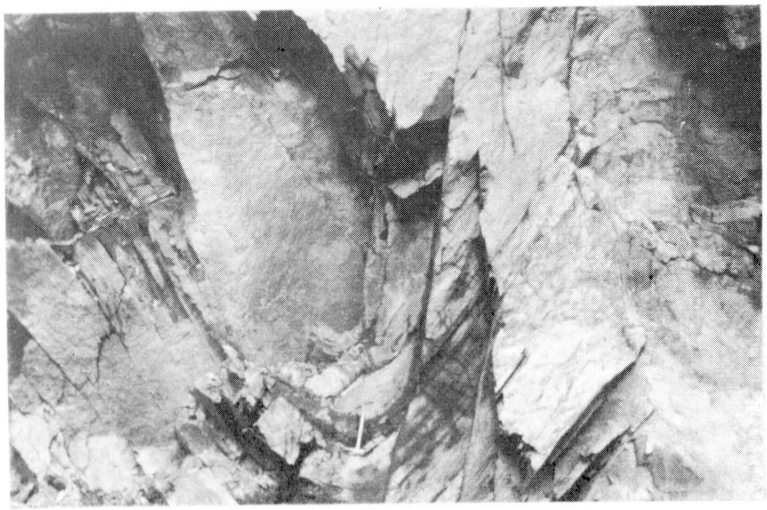

FIG. 3

Explanation of Plate XXX

Fig. 1 Relation between L_m and L_3. The lineation characterized by parallel orientation of amphibole (trending NW-SE in this figure) is bent or flexured by L_3 (trending NE-SW). ×1.

Fig. 2 S_{2-2} and the type III folds are recognized in this figure. In the lower part, the type I folds (rootless) are refolded by the type III folds. ×4.

Fig. 3 Helicitic structures in albite porphyroblasts in spotted pelitic schist from 510m from the entrance in the adit of the Sazare Mine. The structures of dark inclusions are identical with the type I or II folds. ×100.

Fig. 4 A helicitic strucure in a albite porphyroblast in spotted pelitic schist from 1 km north of Fujiwara. The helicitic structure is identical with S_{2-2}. ×100.

FIG. 1

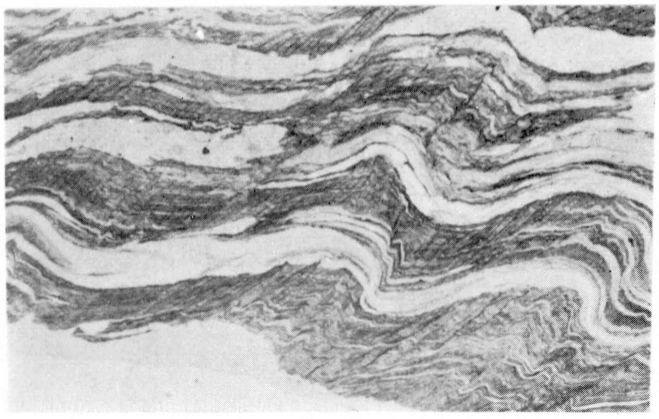

FIG. 2

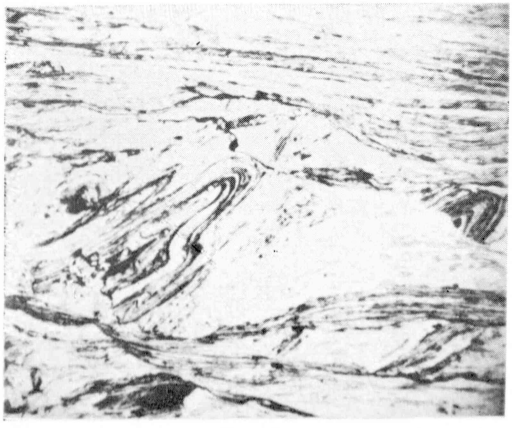

FIG. 3

FIG. 4